Hyaluronic acid/PEO electrospun tube reduces tendon adhesion to levels comparable to native tendons - An in vitro and in vivo study

Miescher, Iris ; Schaffner, Nicolas ; Rieber, Julia ; Bürgisser, Gabriella Meier ; Ongini, Esteban ; Yang, Yao ; Milionis, Athanasios ; Vogel, Viola ; Snedeker, Jess G ; Calcagni, Maurizio ; Buschmann, Johanna

DOI: https://doi.org/10.1016/j.ijbiomac.2024.133193

International Journal of Biological Macromolecules 273 (2024) 133193

Contents lists available at ScienceDirect

International Journal of Biological Macromolecules

journal homepage: www.elsevier.com/locate/ijbiomac

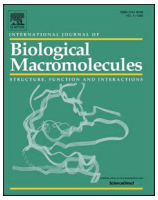

Hyaluronic acid/PEO electrospun tube reduces tendon adhesion to levels comparable to native tendons – An *in vitro* and *in vivo* study

Iris Miescher [a], Nicola Schaffner [a], Julia Rieber [a], Gabriella Meier Bürgisser [a], Esteban Ongini [b], Yao Yang [c], Athanasios Milionis [d], Viola Vogel [e], Jess G. Snedeker [b], Maurizio Calcagni [a], Johanna Buschmann [a,*]

[a] Division of Plastic Surgery and Hand Surgery, University Hospital Zurich, Sternwartstrasse 14, 8091 Zurich, Switzerland
[b] University Clinic Balgrist, Orthopaedic Biomechanics, Forchstrasse 340, 8008 Zurich, Switzerland
[c] Department of Health Sciences & Technology & Department of Materials, Schmelzbergstrasse 9, LFO, 8092 Zürich, Switzerland
[d] Laboratory of Thermodynamics in Emerging Technologies, Department of Mechanical and Process Engineering, ETH Zürich, 8092 Zürich, Switzerland
[e] Laboratory of Applied Mechanobiology, Institute of Translational Medicine, and Department of Health Sciences and Technology, ETH Zurich, 8093 Zurich, Switzerland

ARTICLE INFO

Keywords:
Hyaluronic acid (HA)
Adhesion formation
Tendon repair
Tenocytes, electrospinning
Polyethylene oxide

ABSTRACT

A major problem after tendon injury is adhesion formation to the surrounding tissue leading to a limited range of motion. A viable strategy to reduce adhesion extent is the use of physical barriers that limit the contact between the tendon and the adjacent tissue. The purpose of this study was to fabricate an electrospun bilayered tube of hyaluronic acid/polyethylene oxide (HA/PEO) and biodegradable DegraPol® (DP) to improve the anti-adhesive effect of the implant in a rabbit Achilles tendon full laceration model compared to a pure DP tube. Additionally, the attachment of rabbit tenocytes on pure DP and HA/PEO containing scaffolds was tested and Scanning Electron Microscopy, Fourier-transform Infrared Spectroscopy, Differential Scanning Calorimetry, Water Contact Angle measurements, and testing of mechanical properties were used to characterize the scaffolds. *In vivo* assessment after three weeks showed that the implant containing a second HA/PEO layer significantly reduced adhesion extent reaching levels comparable to native tendons, compared with a pure DP implant that reduced adhesion formation only by 20 %. Tenocytes were able to attach to and migrate into every scaffold, but cell number was reduced over two weeks. Implants containing HA/PEO showed better mechanical properties than pure DP tubes and with the ability to entirely reduce adhesion extent makes this implant a promising candidate for clinical application in tendon repair.

1. Introduction

Tendons consist of dense viscoelastic, fibrous connective tissue and transfer muscle force to bones enabling joint motion. They are hypovascular [1,2] and hypocellular with a low metabolic activity leading to a limited natural healing capacity, frequently resulting in the formation of fibrovascular scar tissue and inferior mechanical properties [3]. Accidents or overuse in daily life or in sports, but also age-related degeneration or adiposity [4] may be risk factors for tendon disease affecting four millions new patients per year worldwide [1,5–7]. Tendons heal in three overlapping phases: Immediately after injury, an inflammatory response occurs including intrinsic and extrinsic pathways lasting for about 3–7 days [8]. In the following repair phase, the injury site becomes hypercellular, characterized by an increase in (myo)fibroblasts and deposition of new extracellular matrix (ECM). After about 6 weeks, the remodeling phase begins replacing the randomly orientated collagen III fibers by collagen I and orientating them in longitudinal direction [9–11]. Although the third phase can last up to one year, quality of the healed tendon remains inferior caused by still decreased fiber orientation and scar tissue with worse biomechanical properties. Several animal models have confirmed these findings [12,13], documenting that repaired tendons reach only 40–70 % of uninjured tendon strength [14–16]. Re-rupture, joint stiffness and adhesion formation are common clinical problems that lead to secondary surgeries, persisting functional

* Corresponding author.
E-mail addresses: iris.miescher@usz.ch (I. Miescher), nicola.schaffner@usz.ch (N. Schaffner), julia.rieber@usz.ch (J. Rieber), gabriella.meierbuergisser@usz.ch (G.M. Bürgisser), esteban.ongini@hest.ethz.ch (E. Ongini), yang.yao@hest.ethz.ch (Y. Yang), athanasios.milionis@ltnt.iet.mavt.ethz.ch (A. Milionis), viola.vogel@hest.ethz.ch (V. Vogel), jess.snedeker@hest.ethz.ch (J.G. Snedeker), maurizio.calcagni@usz.ch (M. Calcagni), johanna.buschmann@usz.ch (J. Buschmann).

https://doi.org/10.1016/j.ijbiomac.2024.133193
Received 19 December 2023; Received in revised form 10 June 2024; Accepted 13 June 2024
Available online 15 June 2024

disability and impairments in patients daily lives [17].

Thanks to animal models and cell-culture based experiments tendon healing processes are better understood, but in the clinics surgery and rehabilitation are still the gold standard so far [10,18]. Rabbit Achilles tendon (AT) and human hand flexor tendons show similar biomechanical properties with nearly the same ultimate failure load [19,20], and although not having a synovial sheath rabbit AT are inclined to develop adhesion formation [20,21]. This makes the rabbit AT full transection a good model for improving the treatment of hand tendon injuries, an important field for plastic surgeons as hand injuries represent 20 % of all injuries treated in emergency [6,22].

An effective method to reduce adhesion formation after surgery is the implantation of porous physical barriers, limiting the contact between the tendon and the surrounding tissue but allowing cytokines, growth factors and metabolic waste to pass without disturbing tendon movement, mechanical properties and the healing process [8,18,23]. Synthetic and biological biomaterials such as DegraPol® based on hydroxybutyrate and Ɛ-caprolactone, a biodegradable and biocompatible polyester urethane [21,24], chitosan-based scaffolds [25], decellularized extracellular matrix (ECM) [26] or Type I collagen-based scaffolds [18,23] have been used in animal models. The polyester urethane DegraPol®15 (DP) utilized in this study has been shown to be a good scaffold material for tenocytes [27], and previous work demonstrated that cellular response in a rabbit full laceration AT model was not impaired while adhesion formation could be reduced by about 20 % [28,29]. In addition, the elasticity of the electrospun DP tube is an advantage for the surgery because the material has a high strain at break compared to other commonly used materials. As adhesion extent in rabbit AT full laceration model has been shown to be reduced with pure DP implants [29] we aimed to improve the electrospun implant by adding hyaluronic acid (HA) to reduce adhesion formation further.

Hyaluronic acid is a major component of the ECM, playing essential roles in cell signaling, wound healing, tissue regeneration and matrix organization [30,31]. It is an important lubricating component of the synovial fluid and supplies the tendon with nutrients [32]. Macrophages and fibroblast-like cells synthesize HA in the synovial membrane [33,34] and its production increases after injuries, which improves cell viability and cell proliferation, and reduces inflammation [30,35–37]. Thanks to the biocompatible and biodegradable properties, HA is often applied in medical therapies and experimental studies [30,31,38,39]. Injections of HA have shown positive effects regarding tendon maturity, strength, stiffness and joint function in animal models [37,40,41] possibly induced by a reduced inflammation. Due to the lubricating properties and the presence in the synovial fluid the application of HA is frequently used with the aim to reduce adhesion after surgery, and collected data show that a repeated administration of sodium hyaluronate may improve the postoperative active finger motion in human [42]. Electrospun core-shell fiber meshes with a poly caprolactone shell and a hyaluronic acid/PRP core have been applied around a rabbit flexor tendon rupture and demonstrated their anti-adhesion effects [43]. A case report on a hyaluronic acid/alginate wrap that was applied around a lacerated *flexor pollicis longus* showed a clear reduction of adhesions when a second inspection was enabled by another injury the following year [44].

Hyaluronic acid is an unbranched glycosaminoglycan with hydrophilic properties [30]. Effects of HA depend on its molecular weight ranging from 5×10^4– 2×10^8 Da [45] and its concentration influencing signaling pathways and differential macrophage activation [30,35,46], viscosity and viscoelasticity [30]. High molecular weight (HMW) HA ($> 10^6$ Da) has been shown to have immunosuppressive, anti-angiogenic and anti-inflammatory effects [47], while low molecular weight (LMW) HA shows opposite effects [48,49]. The balance between HA synthesis provided by hyaluronan synthases and HA degradation by hyaluronidases and oxidative damage caused by reactive oxygen species (ROS) [30,31] is therefore very important. Hyaluronic acid in combination with autografts and allografts is a promising treatment option in wound healing [50,51].Thanks to the 3D nanostructure of electrospun scaffolds [52], their application has been shown to be a good alternative treatment reducing adhesion as well [29]. Additionally, usage of HA in electrospun scaffolds showed positive effects regarding bacterial biofilm formation, bacterial adherence and cell proliferation [50,53]. Rabbit tenocytes supplemented with HMW HA exhibited a general down-regulation of matrix markers *in vitro*, and collagen crosslinking enzyme LOX, suggesting that HA *in vivo* will not provoke a fibrotic reaction but rather prevent scar-like adhesion [54].

Thanks to its biodegradability (half-life in blood stream of 2–5 min. [55]), its biocompatibility and biological functions, there is a big interest in HA containing electrospun scaffolds. However, due to high viscosity, high surface tension, and high electrical conductivity, electrospinning of HA may be challenging [56]. Solvents are often used to decrease viscosity and surface tension to enable electrospinning, however, HA is not soluble in volatile organic solvents [45]. The association of HA with other well processable polymers like poly(vinyl alcohol) (PVA) or polyethylene oxide (PEO) nevertheless enables HA electrospinning while maintaining its biological benefits [57].

In sum, many experimental approaches, including the use of growth factors, bioactive agents [58], stem cells, tissue engineering and optimized suture techniques [59] are undertaken with the goal to enhance tendon repair. Despite encouraging progress in the last decades, the long-term clinical results still need to be optimized [60,61].

In this study, we produced a bilayered electrospun tube containing a layer of pure DegraPol® and a layer of HA/PEO [62] in the ratio 1:1 or 1:4 respectively (Scheme 1A), with the aim to use HA as biolubricant and improve the anti-adhesive effect of the DegraPol® tube used in earlier studies [21,28,29]. Besides HA, PEO has been reported to act as an anti-adhesive when applied in combination with carboxymethylcellulose (CMC) in a CMC/PEO gel around lacerated flexor tendons in zone 2 [63]. To the best of our knowledge, the application of a HA/PEO electrospun membrane – with HA *and* PEO exhibiting anti-adhesive features - and with a second DP layer has not been tested so far. To investigate adhesion and proliferation of rabbit tenocytes on the new scaffolds, cells were seeded on the scaffolds and analyzed with Scanning electron microscopy (SEM) and light microscope after immunostaining. Proliferation dynamics were assessed, using alamarBlue™ assay (Scheme 1B). Tubes with a HA/PEO ratio of 1:1 were switched before surgery and applied in a full laceration AT model [20], resulting in an implant with a HA containing layer facing the surrounding tissue (Scheme 1C). Three weeks after implantation, the adhesion extent of the extracted tendons was analyzed using Picrosirius Red and Hemalaun Sudan staining, and results were compared with tendons treated with non-bioactive DP tubes and native tendons. As a HA/PEO layer was the first time combined with a pure DP layer in electrospun scaffolds, material properties were analyzed with SEM, Fourier-transformed infrared Spectroscopy (FTIR), Differential Scanning Calorimetry (DSC), Water Contact Angle (WCA), and by testing the mechanical qualities (Scheme 1D).

2. Material and methods

2.1. Materials

For electrospinning DegraPol®15 (DP), a biodegradable polyester urethane block copolymer, was kindly provided by Ab Medica, Italy. High molecular weight hyaloronic acid (HA, 1.01–1.8 MDa) was ordered from Lifecore Biomedical (Lifecore Biomedical, #HA 15 M, Chaska, USA) and FITC-labeled HA (1.5 MDa) was delivered by TdB Labs (TdB Labs, #FHA-Se, Uppsala, Sweden). Chloroform (#132950), 1,1,1,3,3,3-hexa fluoro-2-propanol (HFP) (#105228), polyethylene glycol (PEG) (in average 35′000 g/mol) (#81310) and polyethylene oxide (PEO) (in average 600′0000 g/mol) (#182028) were purchased from Sigma-Aldrich (Sigma-Aldrich, Buchs, Switzerland). Solutions for electrospinning were filled in a 5 mL glass syringe (Huberlab, #3.7102.33,

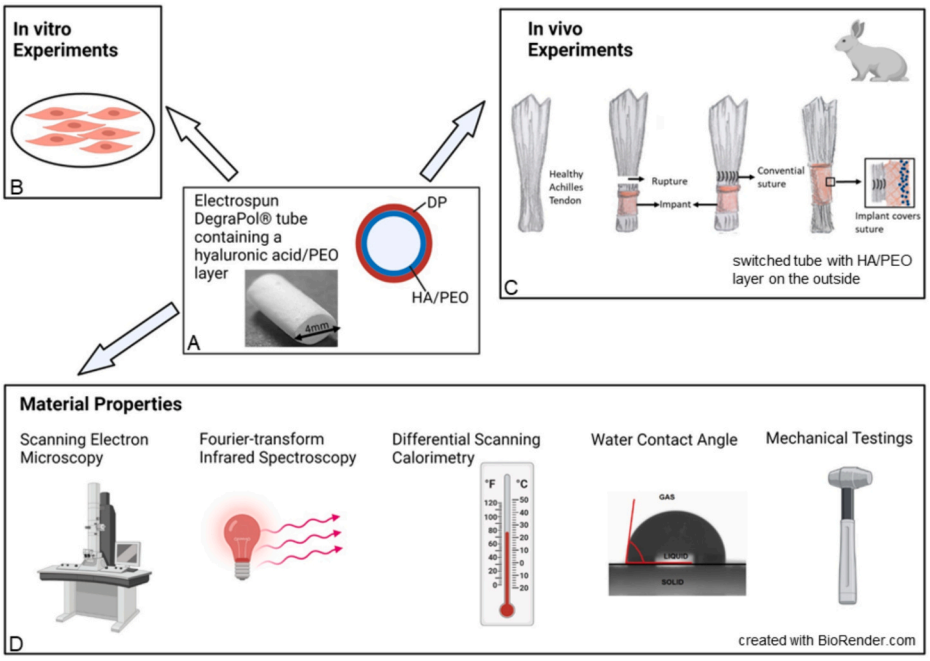

Scheme 1. Experimental procedure. A) Photo and scheme of bilayered electrospun DegraPol® tube with a second layer of HA/PEO in a ratio 1:1 or 1:4. **B)** *In vitro* experiment using rabbit tenocytes seeded on electrospun DP scaffolds with or without a layer of HA/PEO in order to investigate cell adhesion and viability. **C)** Rabbit AT full laceration model, using flipped DP implants that contain a HA/PEO layer in a ratio 1:1, facing the surrounding tissue **D)** Material property analysis of the differently produced electrospun DP tubes with or without HA/PEO by Scanning electron microscope (SEM), Fourier-transform Infrared Spectroscopy (FTIR), Differential Scanning Calorimetry (DSC), static and dynamic Water Contact Angle (WCA) and mechanical tests.

Aesch, Switzerland).

For cell culture, gentamycine (#L0011), Ham's F12 (#L0135–500) and FBS (#S1830–500) were bought from Biowest (Biowest, Nuaillé, France) and amphotericin B from Pan Biotech (Pan Biotech, #P06–01100, Aidenbach, Germany). Penicillin/streptomycin (#15140122) and GlutaMAX™ (#35050038) were delivered from ThermoFisher scientific (ThermoFisher scientific, Basel, Switzerland) and phosphate buffered saline (PBS) from Sigma-Aldrich (Sigma-Aldrich, #D8537, Buchs, Switzerland). Cells were cultured in tissue culture plates from Corning (Corning, PrimariaTM, New York, NY, USA) and alamarBlue™ cell viability assay from ThermoFisher scientific (ThermoFisher scientific, #DAL1100, Basel, Switzerland) was carried out in 12-well plates from Sigma-Aldrich (Sigma-Aldrich, #665180, Buchs, Switzerland) and 96-well plates from Techno Plastic Products AG (TPP,#92,096, Trasadingen, Switzerland).

For immunocytochemical staining an Autostainer Link48 (DAKO, Baar, Switzerland) was used. Target retrieval solution (#GV80411) and washing buffer (#K800721) were ordered from DAKO (DAKO, Baar, Switzerland). Hydrogen peroxide H_2O_2 was bought from Sigma-Aldrich (Sigma-Aldrich, #1.07209.0250, Buchs, Switzerland) and Pertex from Biosystems Switzerland AG (Biosystems, #41–4012-00, Muttenz, Switzerland) was used to fix coverslips. For Collagen I staining a goat polyclonal primary antibody was bought from abcam (abcam, #ab24821, Cambridge, UK; 1:100 dilution), horse anti-goat IgG antibody (H + L) peroxidase was ordered from Biozol (Biozol, #VEC-PI-9500, Eching, Germany) and horse serum from AdipoGen (AdipoGen, #VC-S-2000, Liestal, Switzerland) was used for blocking. For Fibronectin staining a mouse monoclonal primary antibody was purchased from Sigma-Aldrich (Sigma-Aldrich, #F0791, Buchs, Switzerland; 1:200 dilution) and for α - SMA staining a mouse monoclonal primary antibody from DAKO was applied (DAKO, #IR611, Baar, Switzerland,; 1:2 dilution). For Fibronectin and α - SMA staining a peroxidase labeled polymer conjugated to goat anti-mouse immunoglobulins from DAKO was applied (DAKO, #K4001, Baar, Switzerland) and samples were blocked with goat serum from AdipoGen (AdipoGen, #VC-S-1000, Liestal, Switzerland).

To chemically dry scaffolds seeded with tenocytes for SEM, 1,1,1,3,3,3-hexamethyldisilazan (HMDS) from Carl Roth AG (Carl Roth AG, #3840.3, Arlesheim, Switzerland) was used.

2.2. Methods

2.2.1. Solution preparation for electrospinning

A mixture of chloroform/hexafluoropropanol (HFP) (80:20 wt/wt) was used for the preparation of a 12 wt% DP polymer solution at room temperature (RT; 22–25 °C) the day before electrospinning. HA/PEO solutions (2 wt%) without DP were prepared at 1:1 and 1:4 weight ratios and dissolved in MilliQ water under stirring at 500 rpm for 48 h at RT. To fabricate a FITC-labeled HA/PEO 1:1 fiber mesh, a solution consisting of half of the HA powder and half of FITC-labeled HA powder was used. PEG (30 wt%) was dissolved in chloroform at room temperature and used for electrospinning the next day. Polyethylene oxide (PEO) and PEG are both poly ethylene glycol polymers differing in their molecular weight (PEG on average 35′000 g/mol; PEO on average 600′000 g/mol).

2.2.2. Electrospinning

Electrospinning was carried out with an in-house assembled electrospinning device (Fig. S1), consisting of a DC high voltage supply (Glassman High Voltage Inc., High Bridge, NJ, US), a spinning head with a blunt end and a stainless steel tube (1 mm inner diameter and 0.3 mm wall thickness, Angst & Pfister AG, Zürich, Switzerland). The spinning head was fixed on a transporter and connected *via* a Teflon hose with a syringe pump (SP210cZ, WPI, Germany). The solutions were filled in a 5 mL glass syringe and the electrospun fibers were collected on a metal rod with a diameter of 4 mm for rabbit implants or 6 mm for *in vitro* and mechanical experiments fixed to a rotary motor (Euro Star B rotary motor, IKA Labortechnik) rotating with 500 rpm. Flow rate was set at 1 mL/h for all solutions. For PEG and DP solutions, 12.5 kV and a working distance of 18.5 cm were used while layers containing HA/PEO were produced with 20 kV and a working distance of 14 cm. The

electrospinning was performed at RT with an air humidity between 21 − 35 % for PEG and DP, and 21 − 26 % for HA/PEO solutions. Electrospinning times were 130 min for both, DP layers and for HA/PEO layers. In all tubes, a first thin layer consisted of pure PEG facilitating the detachment of the tube from the metal rod because PEG readily dissolves after immersion in 50 % ethanol. The Teflon hose was rinsed with chloroform and dried with air between electrospinning different solutions. Due to the electrospinning on a flat metal rod the inner layer of the tubes possess a smoother surface whereas the outer layer has a rougher surface with tertiary structures such as grooves. For the *in vivo* experiment, a first layer of HA/PEO was electrospun followed by a pure DP layer and tubes were flipped before implantation because a flat HA/PEO surface was required to finally face the surrounding tissue *in vivo*. The scaffolds had two layers containing just one type of fibers, either pure DP fibers or fibers composed of HA/PEO. For the *in vitro* experiments three layered patches were produced with a DP layer in the middle flanked by a HA/PEO layer on each side to ensure cell seeding on a HA/PEO surface. FITC-labeled HA/PEO solution was electrospun on a glass slide fixed to the rotating drum, using the same conditions as for the tube electrospinning.

2.2.3. Scanning electron microscopy (SEM) and fluorescence microscopy

For SEM, electrospun scaffolds were mounted on metal stubs using conducting double-sided tape and were sputter coated with 10 nm platinum (safematic CCU-010, Zizers, Switzerland). For each material three samples ($n = 3$) were analyzed by SEM (Zeiss Gemini 450, Feldbach, Switzerland) at an accelerating voltage of 5 kV using the secondary electron detector. Three different locations per scaffold were captured at 700× magnification and pictures were analyzed with ImageJ (1.53e/Java 1.8.0_172 (64-bit)). To determine fiber thickness a diagonal was drawn on the picture and fibers crossing the line were measured. To measure pore sizes pores on the surface of both diagonals were analyzed. Images from tenocyte seeded scaffolds were captured at an accelerating voltage of 1.5 kV using the secondary electron detector at 5000× magnification and analyzed qualitatively.

To image FITC-HA labeled fibers a confocal microscope equipped with a digital camera was used (LEICA DM6000B, Heerbrugg, Switzerland) and samples were imaged at 200× magnification.

2.2.4. Fourier-transform infrared spectroscopy (FTIR)

Fourier transformed infrared spectroscopy was performed on a Varian 640 Fourier Transform Infrared Spectrometer (FTIR) equipped with a Golden Gate-diamond ATR with temperature control. For the spectra, 64 scans were averaged collected in a wavenumber range of 600 − 4000 cm^{-1} at a resolution of 4 $c\bar{m}^{1}$. Four scaffolds per material ($n = 4$) were used and three regions of each scaffold were scanned. For visual presentation of the data, normalization to the C═O peak at 1720 cm^{-1} was performed using GraphPad Prism 9 for Windows (GraphPad Software, San Diego, California USA). To compare the different materials, the ratios between the C═O peak at 1720 $c\bar{m}^{1}$ and the C—O peaks at 1155 cm^{-1} and 1100 $c\bar{m}^{1}$ were calculated. Corresponding bonds were assigned by comparing the peaks to IR-spectrum table (Merck KGaA, Darmstadt, Germany) and to according literature [58,64–67].

2.2.5. Differential scanning calorimetry (DSC)

Thermal analysis of the samples was carried out using a differential scanning calorimeter, DSC2500 (TA Instruments). Four scaffolds per material (n = 4) in a weight range of 3–15 mg were analyzed. Two heating cycles with an intermediate cooling cycle were performed from −90 °C to 170 °C with a heating and cooling rate of 10 °C/min. To compare the different samples, only the second heating cycle was taken into consideration. The glass transition point and the phase transition enthalpy were calculated with the software of the DSC (TA Instruments TRIOS v5.1.1.46527).

2.2.6. Static and dynamic water contact angles (WCA)

Static and dynamic water contact angles on scaffold surfaces were measured by a video-based optical contact angle measuring instrument (OCA 35 Dataphysics, Germany). For static WCA a drop of 5 μL Milli-Q water was put on the scaffold surface according to reported WCA measurements [68]. The angles on both drop sides were measured for three scaffolds per material ($n = 3$) and measurements were repeated 5 − 10-times per scaffold. The calculated angle mean was defined as static WCA.

For dynamic WCA, the advancing and receding WCAs were measured and hysteresis was calculated by substracting receding WCA from advancing WCA values [69]. To determine the advancing WCA an initial drop of 5 μL Milli-Q water was positioned on the scaffold and was filled continuously with water. Angles were measured when the drop baseline on the scaffold jerkily increased. The receding angle was measured the same way but water was removed from the water drop. To measure the contact angle, a video of the process was taken, the left and right angles were measured using ImageJ (1.53e/Java 1.8.0_172 (64-bit) and averages were calculated. Three samples were used per material (n = 3) and three measurements were carried out per sample.

2.2.7. Mechanical tests

To measure the stress-strain curve of the different materials a uniaxial load test machine (Zwick Z010, 20 kN load-cell, testXpert III; Zwick/Roell, Ulm, Germany) was used and a strain rate of 10 mm/min until failure was applied for all specimens. To perform axial and transverse measurements, samples were cut into rectangular pieces of 2 mm × 18 mm and clamped to a gauge length of 10 mm. For ring measurements, 2 mm specimens were cut and clamped to a gage length of 8 mm. Ultimate tensile stress (UTS), fracture strain and the Young's modulus were determined as the peak stress to failure, strain at failure, and the slope of a linear fit of the stress-stain curve up to 20 % strain respectively. Calculation of mechanical parameters was performed with MATLAB (Release 2021a, The MathWorks, Inc., Natick, MA, USA). Stress was calculated as division of force F by specimen cross sectional area, CSA, (stress = F/CSA) and strain as the percent change in length from the gage length. Young's modulus was assessed as the slope in the linear region of the stress-strain curve. For the HA containing tubes, 3 tubes per material were used and 6 measurements per tube were carried out. For the pure DP tubes, 2 samples with 6 repetitions were measured.

2.2.8. Cell isolation

Rabbit tenocytes were isolated from ATs of three New Zealand White rabbits using the cell migration method (Approval by the veterinary office of Canton Zurich, reference number ZH 080/2021; 33,530). Briefly, tendons were extracted from the animals and washed with PBS supplemented with 200 μg/mL gentamicin and 2.5 μg/mL amphotericin B. Tendons were cleaned from the surrounding tissue and the central part of the tendons was cut into very small pieces (< 2 mm) and washed 3- times in PBS buffer. Afterwards, multiple tissue pieces were placed into a tissue culture plate and a drop of cell culture medium was added onto each tissue piece (Ham's F12, 10 % FBS, 100 U/mL penicillin, 100 μg/mL streptomycin and 1 % GlutaMAX). Tissues were allowed to attach onto the cell culture plates for 2 h at 37 °C and 5 % CO_2 before adding 10 mL of cell culture media into each plate. The plates with the tissues were not moved for the first 5 days, to decrease tissue detachment upon plate movement and to allow cells to start migrating out from the tissues. The first medium change was done after 5 days, and subsequently, the culture medium was changed every third day. After approximately 2 weeks, tissue pieces were removed from the plates, and cells were allowed to proliferate for 1 week more before cryopreservation. Cryopreserved rabbit tenocytes were thawed, resuspended in culture medium and cultured at 37 °C and 5 % CO_2 with media being changed every second day. Tenocytes between passages 2 and 4 (P 2 − 4) were used for all experiments. The same procedure has been reported before [70].

2.2.9. Cell seeding and proliferation assay on scaffolds

Pure DP scaffolds and DP scaffolds containing HA/PEO layers were sterilized with UV for 30 min. on each side. Half of the scaffolds were shortly wetted in 50 % ethanol afterwards, rinsed 3- times with water and washed once with medium before cells were seeded on the scaffold surface in a 12-well plate. Circles of 5 mm diameter were punched out of all different scaffolds and tenocytes from three donors (P 2 – P 3, 1×10^5 cells in 10 μL medium) were seeded on top and allowed to settle at 37 °C and 5 % CO_2 for about 3 h before adding 1 mL cell culture media to each well. The culture media was exchanged every third day and the experiment was carried out in technical duplicates. Cell proliferation was determined on day 3, 7 and 14 by alamarBlue™ cell viability assay. Thereafter, the scaffolds were transferred into a 96-well plate and incubated with 100 μL 1:10 diluted alamarBlue™ solution for 4 h before excitation wavelength of 530 nm and emission wavelength of 590 nm were measured using a Cytation 5 imaging reader (BioTEk, Agilent Technologies AG, Basel, Switzerland). After measurement, scaffolds were washed once with medium before adding 100 μL culture medium for further cultivation. Empty wells were filled with PBS to prevent dehydration. After measurement on day 14, scaffolds were fixed in 4 % paraformaldehyde (PFA) for further immunostaining, respectively, in 0.5 % glutaraldehyde / 3 % PFA for further SEM preparation and stored in the fridge.

2.2.10. Histological analysis and sample preparation for SEM analysis of cell seeded scaffolds

For histological analysis, tenocyte seeded scaffolds were embedded in paraffin according to commonly established protocols and cut into 3 μm thick slices before deparaffinization with xylene and subsequent rehydration. Immunocytochemical staining for collagen I, fibronectin and α - SMA was carried out with standardized protocols, using Autostainer Link48. Briefly, after antigen retrieval samples were exposed to 3 % H_2O_2 for 10 min. After washing with washing buffer, samples were blocked with serum for 30 min and primary antibody was added for 1 h. After the next washing step, samples were treated with HRP for 20 min., washed again and exposed to DAB for 10 min. Then samples were stained with hematoxylin for 10 min. and rinsed with washing buffer before they were transferred into water and dehydrated with ethanol. Slides were imaged for qualitative analysis at 100×, 200× and 400× magnification using a confocal microscope (Leica AF 6000B).

For SEM preparation, tenocyte seeded scaffolds were washed once in PBS and dehydrated in a series of ascending concentration of ethanol (30 %, 50 %, 70 %, 80 %, 95 % (5 min each step) and 100 % (2- times 10 min)). Subsequently, scaffolds were chemically dried in HMDS/ethanol mix (1:3, 1:1, 3:1) and pure HMDS, each step for 15 min). HMDS was allowed to evaporate overnight, and the samples were mounted on SEM stubs. For SEM imaging see preceding section 2.2.3.

2.2.11. In vivo implantation

For the implantation of HA/PEO/DP tubes with HA:PEO in a ratio 1:1, 3 female New Zealand White rabbits, aged 12 − 16 weeks, specific pathogen free (SPF), were used (Charles River, Research Models and Services, Germany). The animals were housed, maintained and fed as previously described [20] and acclimatized to their environment for 2 weeks before surgery. Ethical approval for the experiments was achieved from the veterinary office of Zurich, Switzerland (reference numbers ZH 080/2021; 33530). The full transection of the Achilles tendon 2 cm above the calcaneus, followed by a 4 -strand Becker suture was carried out as described earlier [20]. The tubes were sterilized with H_2O_2 (plasma sterilization) before implantation and flipped over the wound. The tube was flipped inside-out because the smooth inner surface consisting of HA/PEO that had been produced as the first layer on the metal rod should face the surrounding tissue, while the rough surface made of pure DP fibers should face the repaired tendon. Afterwards the wound was closed with a running suture (using a USP 6.0 polypropylene fiber) and a well-padded cast was applied with an angle of 180° at the ankle. The rabbits got a Durogesic Matrix patch after surgery (Janssen-Cilag AG, Switzerland) with 4.2 mg Fentanyl per patch to provide analgesia for about 72 h with 25 μg/h Fentanyl. The rabbits were euthanized three weeks later in deep anaesthesia (100 mg/kg Ketamine and 4 mg/kg Xylazine) with 80 mg/kg Pentobarbital (Esconarkon ad us. vet., Switzerland) and the tendons were removed. Surgery was performed on one hind leg while the counter hind leg was not treated (NT) and served as control. The extracted tendons were immediately frozen and stored at −20 °C in a gauze moistened with 0.9 % NaCl-solution.

2.2.12. Histological analysis of repaired tendons

The tendons were thawed overnight at 4 °C and warmed to RT before they were dehydrated and embedded in paraffin according to commonly established protocols. Cross sections of 5 μm in the wound region (perpendicular to the Achilles tendon) were deparaffinized with xylene and rehydrated prior histological staining with Hematoxylin-Eosin (H&E), Alcian Blue (AB), Hemalaun Sudan (HS), and Picrosirius Red (PS) according to commonly established procedures. To quantify adhesion extent, PS-stained sections in five subsequent cross-sections separated by 2.0 mm as described by Tan et al. (2010) were analyzed at 8× magnification (Leica EZ4D microscope, Switzerland). To calculate the percentage of adhesion, the length of the contact region of the tendon with the surrounding tissue and the whole tendon perimeter were determined with synedra view software (version 22.0.0.12), before dividing the length of the contact region by the length of the total perimeter.

2.2.13. Statistical analysis

Data were analyzed with GraphPad Prism 9 (Version 9.4.0 GraphPad Software Inc., California, US). To test normal distribution Kolmogorov-Smirnov and Shapiro Wilk tests were applied. For normally distributed data or results with a high number of data ($n > 30$), a one-way analysis of variance (ANOVA with Tukey's multiple comparisons test) was used. Not normally distributed results were analyzed with the nonparametric Kruskal-Wallis test. *P*-values ≤0.05 were considered significant and denoted with an asterisk within graphs ($*p \leq 0.05$; $**p \leq 0.01$; $***p \leq 0.001$, and (ns) for non-significant). Calculations were performed in Excel (2016 (16.0.5332.1000) MSO (16.0.5278.1000) 32-bit).

3. Results

3.1. Microfibrous scaffold characterization using scanning electron microscope images (SEM)

Double layered scaffolds containing one layer of pure DP and a layer of HA/PEO in a ratio of 1:1 or 1:4, respectively, were successfully produced using the protocol from Vitkova et al. [62] and from Evrova et al. [58] for the pure DP electrospinning (without HA/PEO). Surfaces of the inner layer of HA/PEO containing DP scaffolds were compared to the inner layer of pure DP scaffolds using SEM images (Fig. 1A), showing a network of random fibers with a diameter of about 6 μm in average in every material (HA/PEO (1:1) 6 μm ± 3 μm, HA/PEO (1:4) 7 μm ± 3 μm, DP 7 μm ± 3 μm) (Fig. 1B). More than half of the fibers had a diameter within 5 − 10 μm, about a third of the fibers showed smaller diameters and only about 10 % of the fibers possessed a diameter larger than 10 μm (Fig. 1B). The significant differences in fiber thickness can be explained by the large number of analyzed fibers ($n = 411$ for HA/PEO (1:1), $n = 737$ for HA/PEO (1:4) and $n = 1178$ for DP). Pore sizes of scaffolds containing HA/PEO were significantly larger than in pure DP scaffolds that did not contain any HA/PEO; with HA/PEO (1:1) 15 μm ± 6 μm, HA/PEO (1:4) 16 μm ± 7 μm and DP 10 μm ± 6 μm (Fig. 1C). Nearly 60 % of the pores in HA/PEO containing scaffolds showed a diameter of 10 − 20 μm, 3- times more pores than in DP scaffolds in which about 70 % of the pores were smaller than 10 μm (Fig. 1C). Image of a HA/PEO mesh in a 1:1 ratio with FITC-labeled HA proves that high molecular HA is

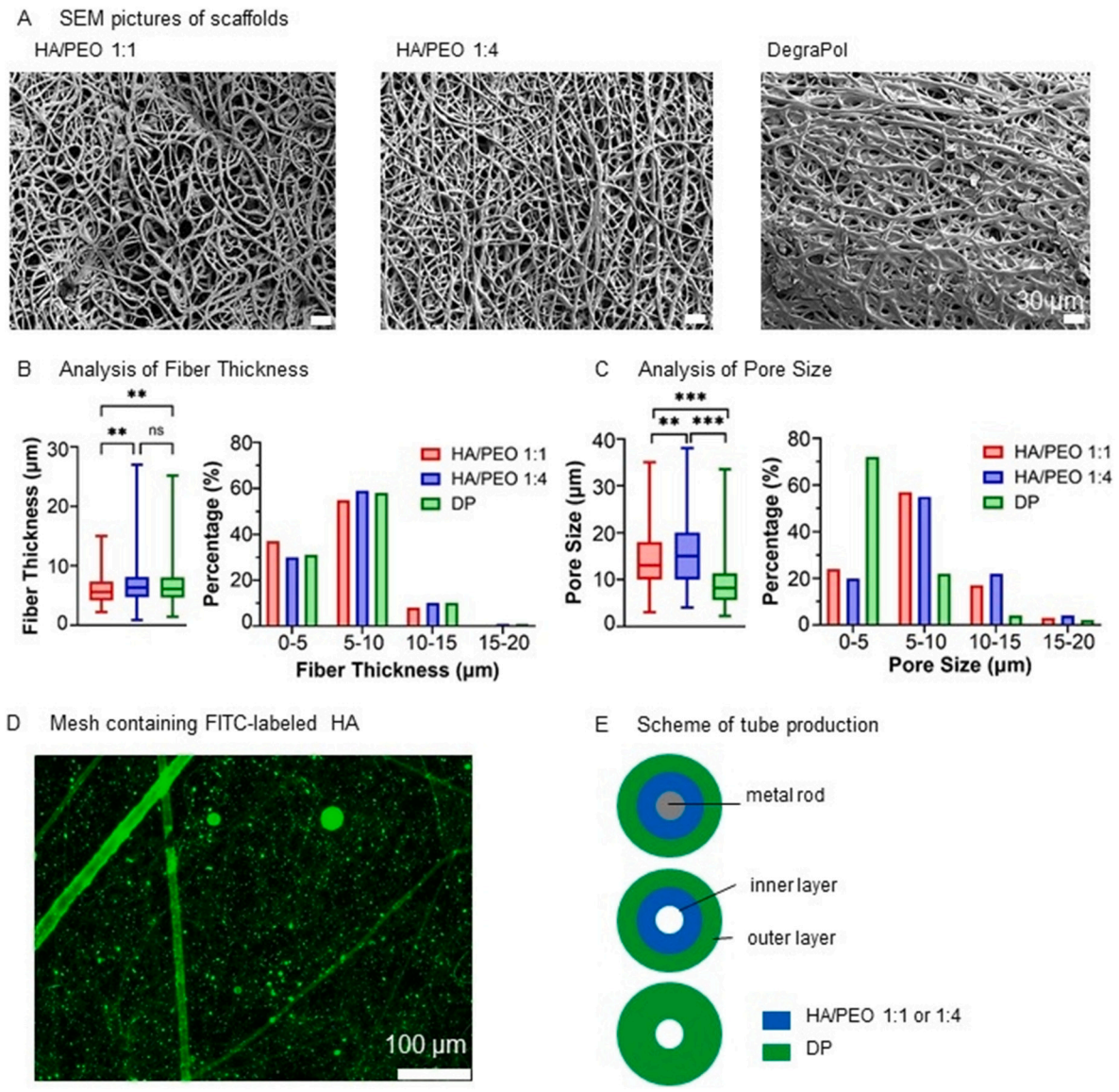

Fig. 1. Analysis of scanning electron microscope images regarding fiber thickness and pore size of DP scaffolds containing a HA/PEO layer and pure DP scaffolds. A) SEM images of differently produced scaffolds. Scale bars: 30 µm **B)** Analysis of the inner scaffold layer consisting of HA/PEO in a ratio 1:1 or 1:4 or pure DP scaffold, fiber thickness (**B**) and pore size (**C**) were assessed. **D)** Image of a HA/PEO 1:1 ratio mesh containing FITC-labeled HA at a 200× magnification. **E)** Scheme of double layered tubes with an inner HA/PEO and an outer DP layer or single layered DP tubes before or after removing from the metal rod. Number of tubes $n = 3$ for all HA containing scaffolds, $n = 6$ for fiber analysis of DP scaffolds and n = 3 for pore size DP scaffolds analysis. An ordinary one-way-ANOVA for each surface was performed (Tukey's multiple comparisons test) to determine significant median differences. Data are shown as box and whisker plots with interquartile range and 95 % confidence interval. *p*-values ≤0.05 were considered significant and denoted with (*), for *p*-values ≤0.01 (**), *p*-values ≤0.001 (***) and for non-significant (ns) was used. Numbers of fibers analyzed to determine fiber thickness HA/PEO (1:1) $n = 411$; HA/PEO (1:4) $n = 737$; DP $n = 1178$. Numbers of pores measured to determine pore size HA/PEO (1:1) $n = 490$; HA/PEO (1:4) $n = 797$; DP $n = 95$.

spinnable, as a fluorescent fiber network could be detected with fluorescence microscopy (Fig. 1D). Schematic structure of electrospun tubes is visualized in Fig. 1E.

3.2. Static and dynamic water contact angle (WCA) measurements

The static WCA provides information about the wettability of materials and is lower than 90° for hydrophilic surfaces, whereas hydrophobic surfaces show WCAs higher than 90°. Although HA is highly hydrophilic, static WCAs of HA containing scaffolds were only slightly lower than values of DP scaffolds and were not significantly different with values of about 100°, classified as moderately hydrophobic material (HA/PEO (1:1) = 100.1° ± 7.5°, HA/PEO (1:4) = 99.5° ± 5.1°, DP = 107.6° ± 4.7°) (Fig. 2A).

Contact angle hysteresis (CAH) is calculated by subtracting the receding contact angle from the advancing contact angle. High CAH values are attributed mainly to surface heterogeneity and roughness [69,71,72]. For the dynamic measuring, all different materials show low receding WCAs and high advancing WCAs leading to high hysteresis (Fig. 2A), with minimally lower values for pure DP material (HA/PEO (1:1) 91.6° ± 0.8°, HA/PEO (1:4) 91.9° ± 3.4°, DP 87.8° ± 3.6°).

3.3. Analysis of Fourier-transform infrared spectroscopy (FTIR)

Fourier-transform Infrared Spectroscopy was assessed for bilayered DP/HA/PEO tubes and single layered DP tubes (Fig. 2B). Additionally, FTIR spectra of a HA/PEO 1:1 mesh with a thinner DP layer, electrospun HA/PEO, electrospun PEO and HA powder were measured. Every DP

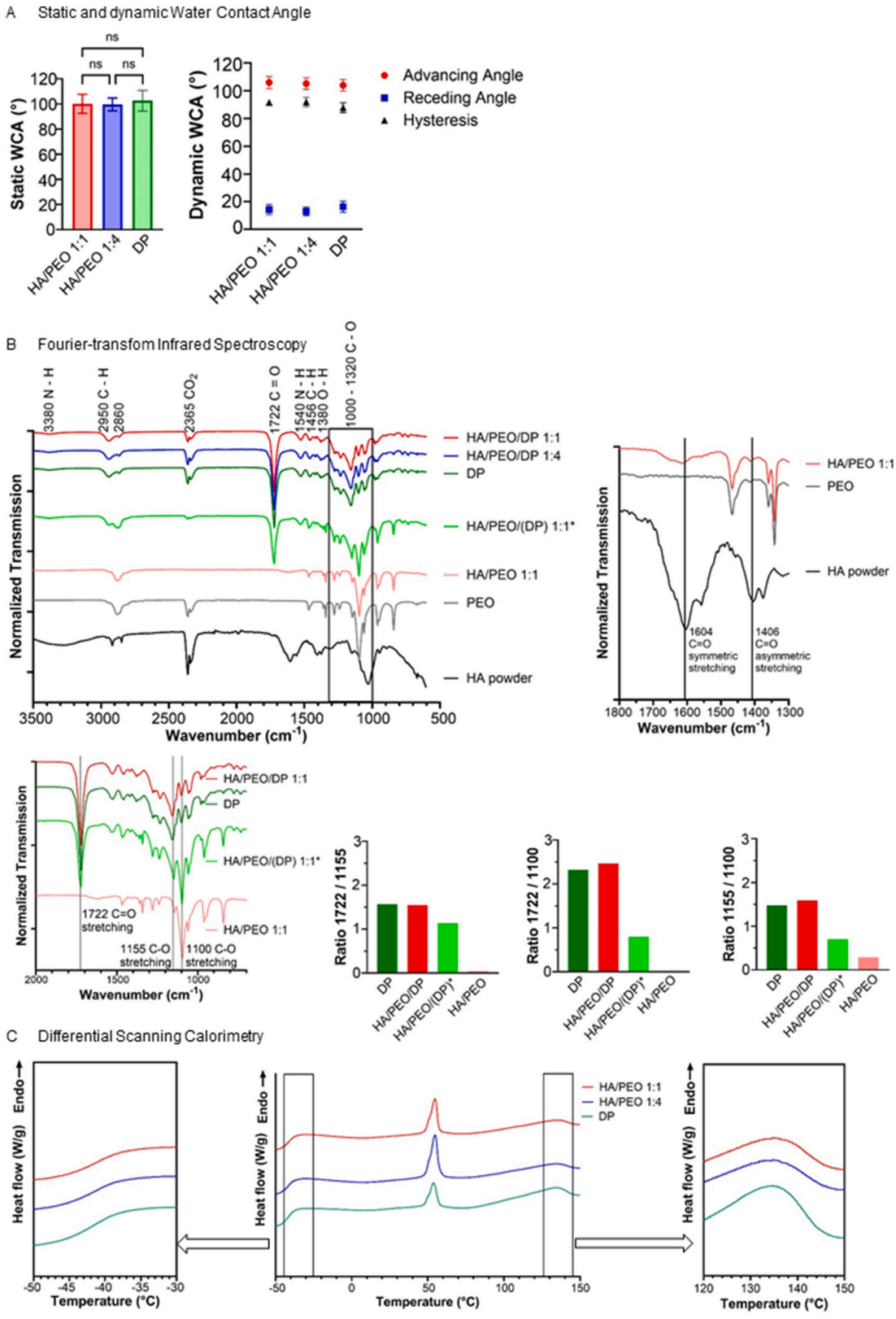

(caption on next page)

Fig. 2. Analysis of Water Contact Angles (WCA), Fourier-transform Infrared Spectroscopy (FTIR) and Differential Scanning Calorimetry (DSC) of scaffolds **A)** Static and dynamic WCA measurements of the inner surface or HA containing scaffolds or pure DP scaffolds. Hysteresis = advancing WCA – receding WCA. Number of tubes / scaffold material $n = 3$. Number of static WCA measurements/scaffold material $n = 50$, number of dynamic WCA measurements/scaffold material $n = 18$ for advancing WCA and $n = 17$ for receding WCA. An ordinary one-way-ANOVA for each surface was performed (Tukey's multiple comparisons test) to determine significant median differences applying 95 % confidence interval. p-values ≤0.05 were considered significant and denoted with (*), for p-values ≤0.01 (**), p-values ≤0.001 (***) and for non-significant (ns) was used. **B)** FTIR absorbance spectra of HA/PEO containing scaffolds, HA/PEO/(DP)* with a thinner DP layer than DP/HA/PEO tubes (electrospinning of DP only for 15 instead of 130 min.), compared to pure DP scaffolds, electrospun HA/PEO, electrospun PEO and HA powder. Four scaffolds were used per material ($n = 4$) and 3 technical replicates were performed for every sample (measurements per material $n = 12$). Spectra have been vertically shifted for visual clarity. For FTIR spectra of each scaffold, see Fig. S2. Region of 1300–1800 $c\bar{m}^1$ is enlarged in a separate spectrum for better visibility of HA-induced peaks. For the detailed HA and PEO spectrum see Fig. S3. Prominent peaks assigned to C═O and C—O junctions are shown in the graph below and corresponding ratios are represented in bar charts. **C)** DSC thermograms of mean values of different scaffolds and enlarged areas of glass transition temperature (T_g) on the left and melting point (T_m) on the right. For DSC thermograms of each scaffold, see Fig. S4. Number of tubes / scaffold material $n = 4$. Thermograms have been vertically shifted for visual clarity.

containing material expressed a prominent peak at 1722 cm^{-1} assigned to the carbonyl group (C═O stretching) of DP [58]. The larger region at 1300–1000 $c\bar{m}^1$ is associated with symmetric and asymmetric stretching vibrations of different C—O bonds and was prominent for DP and PEO containing material although peak intensities varied as can be seen in the small FTIR spectrum below and in the bar charts showing the ratios referring to the wavenumber 1722 $c\bar{m}^1$, 1155 cm^1 and 1100 cm^{-1}. Spectra of single layered DP tubes and DP/HA/PEO tubes looked very similar what was confirmed by the ratios in the bar charts. Reducing the layer of DP in HA/PEO/(DP) tubes led to a similar peak pattern but peak intensities differed slightly resulting in different ratios in consequence indicating the presence of HA/PEO in the tubes. To check whether HA is detectable in HA/PEO electrospun material FTIR of electrospun HA/PEO was compared with electrospun PEO and HA powder. Bonds of C═O present in HA powder changed the spectra of HA/PEO compared to PEO slightly as peak intensity at 1604 cm^{-1} was 3.5- times stronger and at 1406 cm^{-1} 1.5- times stronger than in PEO [64–67]. For detailed FTIR spectrum of HA/PEO, PEO and HA see Fig. S3. The peaks at 2940 cm^{-1} and 2860 cm^{-1} correspond to stretching vibrations of $–CH_2$ and $–CH_3$ groups, while the small peak at about 3380 cm^{-1} is associated with NH stretching. In contrast, the peak at 2360 cm^{-1} results from free CO_2 in the device during measurement.

3.4. Thermal analysis by differential scanning calorimetry (DSC)

Thermograms to determine glass transition temperature (T_g) of amorphous material and melting point (T_m) of crystalline components were assessed using DSC [73] (Fig. 2C). Compared to the pure DP mesh, a mesh with a second layer composed of HA/PEO did not change the typical thermal pattern of DP with a T_g at about −40 °C and a T_m at around 130 °C. The prominent endothermic peak at about 56 °C corresponds to T_m of PEG, used as first thin layer to facilitate removal of the tube from the metal, or to PEO respectively, having the same chemical structure as PEG but a higher molecular weight and is enabling electrospinning of HA..

3.5. Mechanical properties

Mechanical properties such as ultimate tensile stress (UTS), fracture strain and Young's Modulus were tested in the axial and transverse direction of the different scaffolds to determine possible mechanical differences due to the presence of HA and PEO (Fig. 3). Transverse direction measurements were performed either in a ring piece or in a rectangle of an opened tube (Fig. 3A). For UTS, values of HA/PEO containing tubes were 2–3- times higher compared to pure DP tubes, independent of the direction and method; while results of the two HA

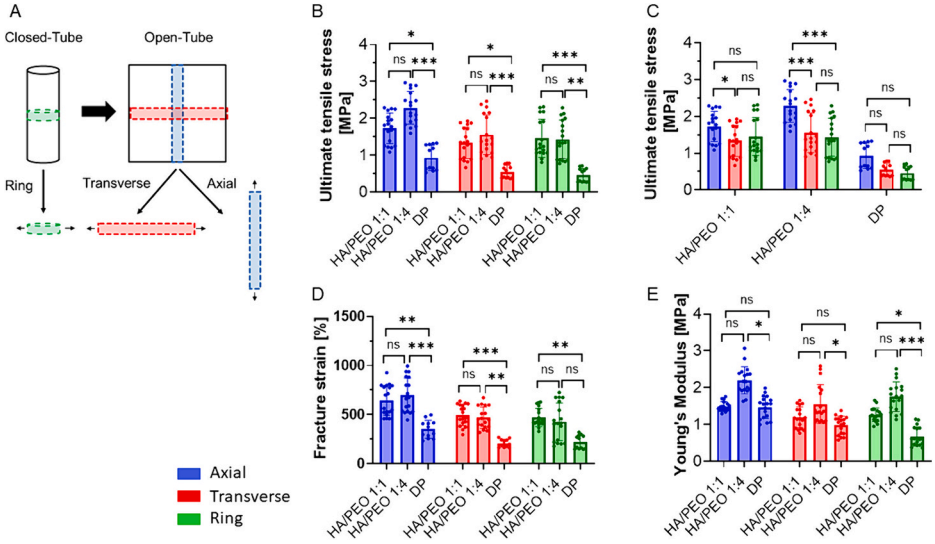

Fig. 3. Mechanical properties of HA containing tubes and pure DP tubes A) Experimental assessment for axial, transverse and ring measurements. **B)** Ultimate tensile stress (UTS) comparing the different materials. **C)** UTS comparing the different measurements in the same material. **D)** Fracture strain and **E)** Young's modulus comparing the different scaffold materials. Data are shown as mean and SD with individual values. Tubes per HA containing material $n = 3$ and pure DP tube $n = 2$, performing 6 measurements per sample. Normal distribution was checked with D'Agostino & Pearson ($\alpha = 0.05$). Kruskal-Wallis test was performed to compare the different tubes (Fig. 3B, D, E) and the different methods for pure DP in Fig. 3C. Due to given normal distribution within HA containing tubes in Fig. 3C, an ordinary one-way-ANOVA was carried out to compare different behavior (Tukey's multiple comparisons test) applying 95 % confidence interval. In all graphical layouts p-values ≤0.05 were considered significant and denoted with (*), for p-values ≤0.01 (**), p-values ≤0.001 (***) and for non-significant (ns) was used. In addition, mechanical properties of wetted and hydrated samples were assessed in the axial direction (Supporting Information **Fig. S5**).

containing tubes with different HA/PEO concentrations showed comparable results with slightly higher values in the axial direction for the ratio 1:4 (Fig. 3B) (mean values axial measurements [MPa]: HA/PEO (1:1) 1.73 ± 0.41, HA/PEO (1:4) 2.29 ± 0.44, DP 0.93 ± 0.35; transverse measurements [MPa]: HA/PEO (1:1) 1.34 ± 0.42, HA/PEO (1:4) 1.56 ± 0.54, DP 0.55 ± 0.18; ring measurements [MPa]: HA/PEO (1:1) 1.46 ± 0.52, HA/PEO (1:4) 1.43 ± 0.52, DP 0.46 ± 0.19). Comparing UTS in the same material, HA/PEO tubes with a ratio of 1:4 showed 1.5 -times higher values in the axial direction than in the transverse direction. For tubes with a ratio of 1:1 only axial compared to transverse measuring was significantly higher (1.3 -fold) but not compared to values obtained by ring measurements. Axial results of DP tubes were higher than transverse results but not significantly different (Fig. 3C).

Similar results can be observed for fracture strain measurements showing no or only moderate difference between HA containing tubes but achieving 2- times higher values compared to pure DP tubes (Fig. 3D) (mean values axial measurements [%]: HA/PEO (1:1) 647 ± 153, HA/PEO (1:4) 670 ± 177, DP 350 ± 91; transverse measurements [%]: HA/PEO (1:1) 495 ± 108, HA/PEO (1:4) 468 ± 108, DP 208 ± 39; ring measurements [%]: HA/PEO (1:1) 471 ± 93, HA/PEO (1:4) 427 ± 191, DP 220 ± 70).

In the Young's modulus DP tubes show the lowest values, but only the HA containing tube in a ratio 1:4 reaches significantly higher values compared to pure DP material, about 1.5 -times higher for axial and transverse measuring and double as high results for ring measurements (Fig. 3E). Consistently, comparing results from both HA containing tubes results are not significantly different although values from tubes with the ratio 1:4 are in tendency higher (mean values axial measurements

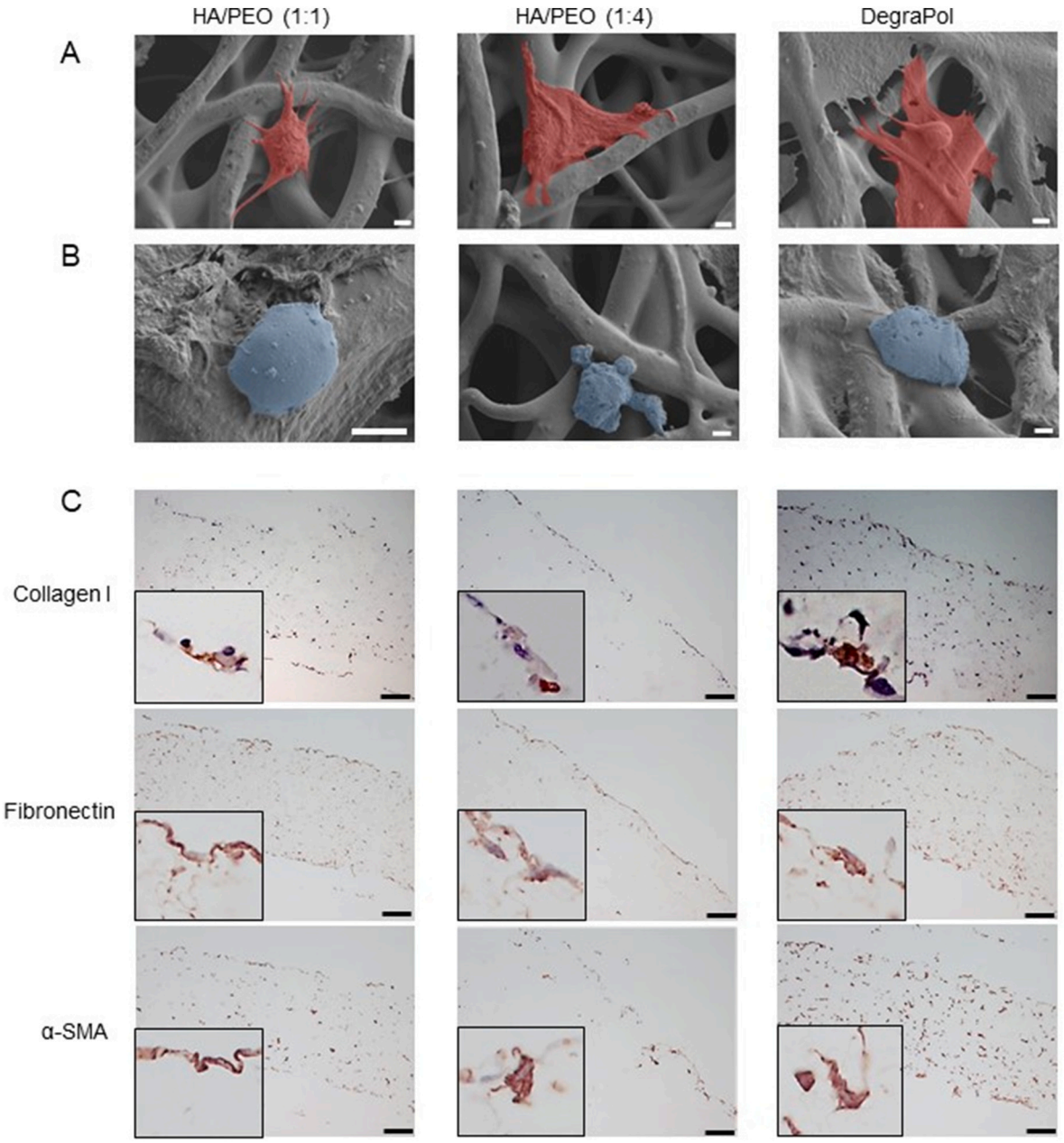

Fig. 4. Qualitative analysis of tenocytes seeded on scaffolds SEM images of tenocytes seeded on different scaffold material. **A)** Long shaped and well attached tenocytes. For better visibility tenocytes are colored in red. **B)** Rounded and less adherent tenocytes. For better visibility tenocytes are colored in blue. Scale bars: 3 μm. **C)** Immunocytochemical staining of tenocyte seeded scaffolds 100× magnified. Scale bars: 100 μm. Integrated small images show tenocytes at higher magnification (zoom into 400× magnified image). For negative controls see Fig. S7.

[MPa]: HA/PEO (1:1) 1.49 ± 0.13, HA/PEO (1:4) 2.2 ± 0.40, DP 1.45 ± 0.37; transverse measurements [MPa]: HA/PEO (1:1) 1.19 ± 0.28, HA/PEO (1:4) 1.56 ± 0.52, DP 0.92 ± 0.28; ring measurements [MPa]: HA/PEO (1:1) 1.26 ± 0.18, HA/PEO (1:4) 1.76 ± 0.40, DP 0.79 ± 0.23). To test whether HA in the electrospun tube is able to absorb water and changing mechanical properties in consequence, a dry bilayered DP/HA/PEO tube with a HA/PEO ratio 1:1 was compared to wetted tubes, sprayed with PBS before stretching, and hydrated tubes, placed into PBS for 80 min. before stretching. No significant differences could be observed when specimen were stretched and recorded in the axial direction (Fig. S5).

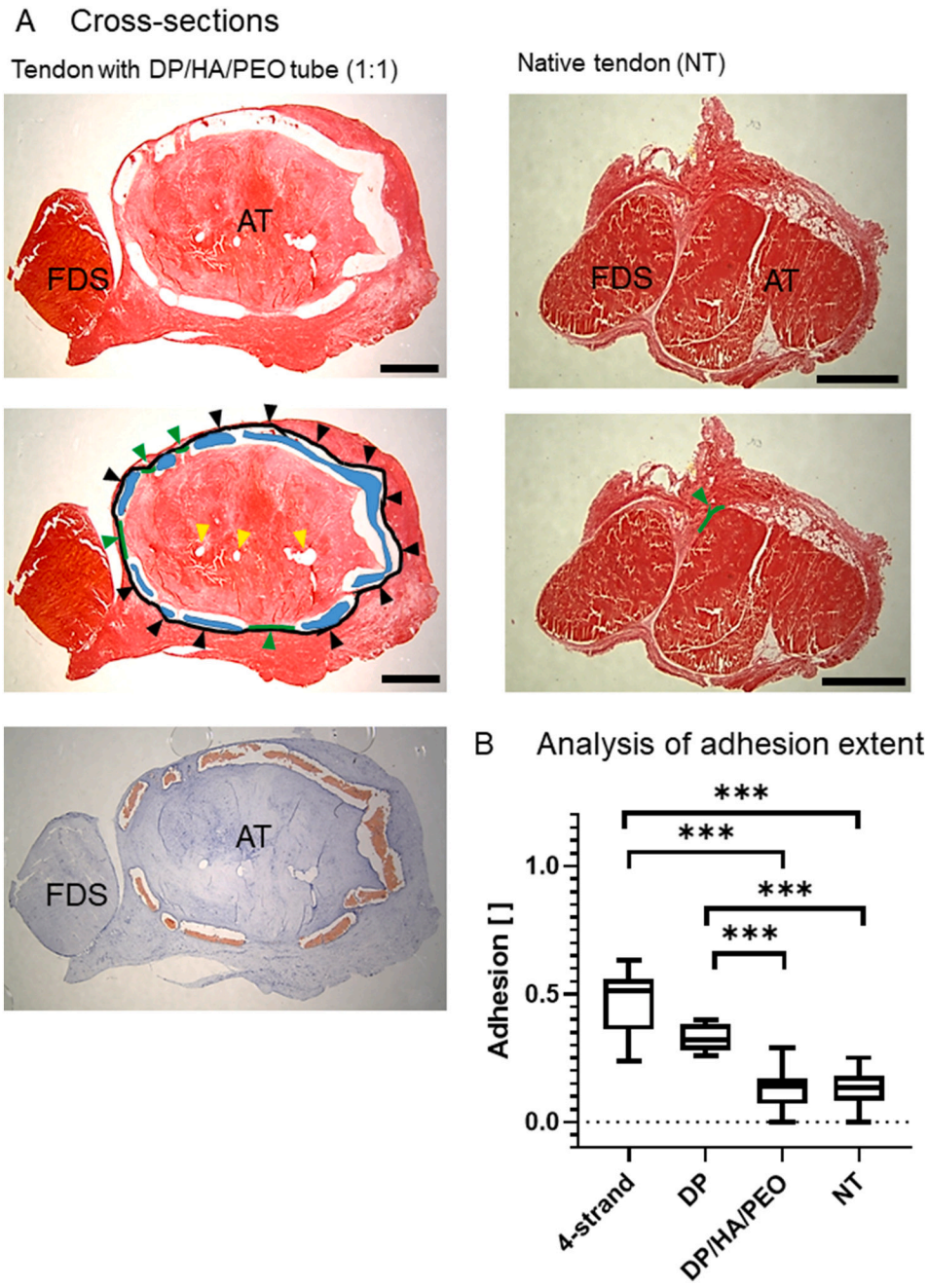

Fig. 5. Assessment of adhesion A) Picrosirius Red stained cross-sections of rabbit Achilles tendon (AT) treated with a DP/HA/PEO tube 3 weeks post-surgery and of native rabbit AT. *Flexor digitorum superficialis* (FDS) is also visible. The DP/HA/PEO tube is schematically indicated in blue color; in the Hemalaun Sudan stained section, the tube is visible in a reddish/orange color. Black arrows label non-adhesive tissue, while green arrows mark adhesion to surrounding tissue. Yellow arrows in the middle of AT are pointing at holes caused by the 4 -strand suture. Scale bar = 1 mm. **B)** Percentage of adhesion extent calculated based on histology, dividing length of adhesion (green line) by total tendon circumference (black line) in 5A. Results from 4 -strand sutured tendons with or without DP implant respectively, were taken from an earlier publication [29] for direct comparison, where the pure DP tubes had been switched before implantation to provide the smooth DP surface towards the surrounding tissue. Data are shown as box and whisker plots with interquartile range and 95 % confidence interval. Rabbits used per treatment: $n = 6$ for 4 -strand sutured tendons and DP treated tendons; $n = 3$ for DP/HA/PEO treated tendons and native tendons (NT). Analyzed sections per treatment: $n = 11$ for 4 -strand sutured tendons and DP treated tendons; $n = 46$ for DP/HA/PEO treated tendons and $n = 32$ for native tendons (NT). Kruskal-Wallis test was performed applying 95 % confidence interval. In all graphical layouts p-values ≤ 0.05 were considered significant and denoted with (*), for p-values ≤ 0.01 (**), p-values ≤ 0.001 (***).

3.6. Cell adhesion, ECM production and proliferation of rabbit tenocytes in vitro

SEM images of cell seeded scaffolds show that tenocytes are able to attach to the fibers of HA/PEO containing bilayered scaffolds and pure DP scaffold. Different shapes and cell morphologies were observed on every scaffold type after two weeks. Not all tenocytes were long shaped and nicely attached to the fibers (Fig. 4A) but roundish, less adherent tenocytes were detected on every scaffold material as well (Fig. 4B). Immunostainings for Collagen I, Fibronectin or α-smooth muscle actin (α - SMA) demonstrated that tenocytes were able to invade the scaffolds and to produce ECM after a 2-week period (Fig. 4C). For all markers strongest staining was observed on pure DP scaffolds and weakest on HA/PEO in a ratio 1:4. In general, only few cells produced Collagen I while many cells expressed Fibronectin and α - SMA, resulting in a stronger staining. AlamarBlue™ staining confirmed adhesion of the tenocytes to the scaffolds on day 3. On 50 % ethanol pre-treated scaffolds cell seeding resulted in higher amount of adhered tenocytes compared to not pre-treated scaffolds, but cell number decreased over time. In contrast, less tenocytes attached to the fibers of not pre-treated scaffolds, but tenocytes were able to proliferate between day 3 and day 7 before cell number decreased (see Fig. S6).

3.7. Effect of HA/PEO tubes on adhesion formation in rabbit full laceration AT model

The effect of the HA/PEO layer in bilayered tubes with a ratio 1:1 in the full laceration AT model was evaluated by histological analysis of the near contact region between the tendon and the surrounding tissue 3 weeks after surgery (Fig. 5). Results were compared with native tendons and with earlier results from repaired tendons with or without pure DP tube implantation [29]. Large areas of non-adhesive tissue can be seen on sections of tendons with a bilayered DP/HA/PEO tube and although HA/PEO layer was directed towards the surroundings during implantation, anti-adhesive effects can be observed as well on the inner tube layer facing the tendon tissue (Fig. 5A). While pure DP tubes decreased adhesion extent in 4 -strand sutured tendons by about 20 % in comparison with sutured tendons without tube [29], application of HA/PEO containing DP tube reduced adhesion of sutured tendons significantly by about 50 % compared to sutured tendons treated with pure DP implants and reached adhesion levels comparable to native tendons (Fig. 5B). Adhesion visible in native tendon is probably a technical artefact caused by the cutting process.

4. Discussion

Tendon healing is a long-lasting process, and natural regeneration capacity of tendons is limited due to their hypovascularization, the dense connective tissue, low cell density and slow cell metabolism. In addition, re-rupture and adhesion formation are common clinical problems after surgery [22,74,75]. Adhesion results from the generation of fibrotic tissue between the tendon and the surroundings and may impair tendon gliding, leading to joint stiffness and pain in up to 30 % of flexor tendon injuries [11]. The detailed mechanism of adhesion formation is still unclear, but persistent inflammation is known to activate fibrogenesis leading to an excessive accumulation of ECM components, such as collagen and alpha smooth muscle actin (α - SMA) [76,77].

Post-operative mobilization with moderate mechanical load [78] has been shown to reduce adhesion extent, but also drugs [78], growth factors [60], and physical barriers have been used for that purpose [29,79]. Because adhesion correlates with compromised tendon gliding capacity, application of biolubricants, for instance HA, is another interesting therapeutic approach [80] as HA is biocompatible and a key component of synovial fluid, ensuring good lubrication of synovial joints [81]. Hyaluronic acid is involved in several important biological processes, such as wound healing and tissue regeneration, cell signaling or matrix reorganization, but its effect depends on many factors, such as concentration and molecular weight. While high molecular weight (HMW) HA has been shown to have immunosuppressive, anti-angiogenic and anti-inflammatory effects, low molecular weight (LMW) HA shows opposite outcomes [30]. So for our aim to reduce adhesion formation, a HMW HA seemed more appropriate than a LMW HA.

Promising results were obtained from the combination of mechanical with biological approaches by adding anti-adhesive HA into scaffold materials, although no such product is available for routine use in clinical practice so far [79]. Electrospun tubes of polycaprolactone alone [43] or in combination with chitosan [50] or acrylate endcapped urethane precursor [82], Zein [53,83] or PEO [84] have been used in combination with HA, showing promising results, but demonstrating that further investigation is necessary. Another successfully electrospun and commercially available material is DegraPol®, a biodegradable and polyester urethane. No adverse reactions of the tendon tissue following tube implantation in a full laceration rabbit AT model was observed [21,24], but adhesion extent was reduced by about 20 % [20,29].

The aim of this study was to improve the anti-adhesive properties of pure DP tubes [29,58], making use of the reported positive anti-adhesive effects of HA in a rabbit full laceration model. Previous results, using HMW HA on tenocytes *in vitro*, have demonstrated that HMW HA did not influence cell proliferation and might have a positive effect on gene expression of some relevant ECM markers. In consequence, HMW HA should not improve fibrotic reaction *in vivo*, but rather avoid adhesion formation [85]. As scaffolds consisting of one pure DP layer and one HA/PEO layer had not been realized before and provide a novel surgical anti-adhesion approach, the new material was characterized by SEM, static and dynamic WCA, DSC thermograms and FTIR, mechanical properties, and by seeding rabbit tenocytes on corresponding scaffolds. The combination of HA as biolubricant with PEO led to stable electrospun fibers, which would not have been achieved with HA alone. PEO furthermore is a non-toxic, biodegradable polymer and dissolves, which facilitates cell detachment and enables anti-adhesion.

Fluorescence microscopy of electrospun FITC-labeled HA demonstrated that high molecular HA in combination with PEO is electrospinnable (Fig. 1D). Analysis of SEM images showed a network of fibers with a diameter of about 6 μm in average in pure DP scaffolds as well as in DP/HA/PEO scaffolds independent of the HA/PEO ratio (Fig. 1B) confirming values of DP fibers published by Rieber et al. [86]. Many factors like humidity, temperature, viscosity or jet stability of the spinneret influence electrospinning outcome, which may lead to differently pronounced morphology of the electrospun material despite constant voltage and flow rate. A possible result of such influences is the high variability of fiber thickness, leading to a large standard deviation, which is most prominent in the HA/PEO tubes with a ratio 1:4. Although average of fiber diameters in every material is similar, statistical analysis showed significant differences between the materials because of the large number of analyzed fibers (HA/PEO (1:1) $n = 411$; HA/PEO (1:4) $n = 737$; DP $n = 1178$). Consistently, distribution of fiber diameter is similar for all meshes with more than half of the fibers having diameters ranged from 5 − 10 μm, about a third of the fibers showing smaller diameters and only about 10 % of the fibers possessing a diameter larger than 10 μm (Fig. 1B). In contrast to the comparable results for fiber thickness, pore sizes of scaffolds containing HA/PEO were significantly larger than in pure DP scaffolds (Fig. 1C) with nearly 60 % of the pores having a diameter of 10 − 20 μm in HA/PEO containing scaffolds, whereas 70 % of the pores in DP scaffolds were smaller than 10 μm (Fig. 1C). The different viscosity, conductivity or surface tension of the HA/PEO solution or the higher voltage and the shorter distance to the metal rod during electrospinning might cause the larger pore diameters in HA/PEO fiber networks [87]. Pore size in HA/PEO containing tubes with a ratio 1:4 showed slightly larger pore diameters than pores in tubes with ratio 1:1 (15.8 μm compared to 14.5 μm), consistent with results from Chen et al. [88]. This demonstrates that increasing amount

of PEO increased pore size in the electrospun PCL scaffolds, possibly influenced by the higher viscosity of the more concentrated PEO solutions. Although pore size has been shown to play a role in cell attachment [84] in our study tenocyte adhesion was similar between the different scaffolds. This might be explained by the fact, that pore sizes of the different scaffolds were still similar despite the statistical difference. AlamarBlue™ experiments demonstrated that tenocytes attached to every scaffold material (randomly provided rough and smooth surfaces), but a decreasing cell number over time was visible, although control cells on plastic proliferated well. These observations are consistent with results from Evrova et al. demonstrating that tenocytes on electrospun DP scaffolds showed a decreased proliferation compared to tenocytes on glass coverslips [87]. Previous studies have shown that a lower fiber/network stiffness correlates positively with cells recruiting nearby fibers resulting in an increased local adhesive ligand density, proliferation and cell spreading [89], therefore a possible explanation might be that tenocytes seeded on single layered DP scaffolds or double layered HA/PEO/DP scaffolds sensed a dense fiber network reducing the number of cells in consequence. Limited permeability for nutrition, oxygen and metabolic waste might be additional factors reducing cell number in the scaffold over 14 days [84].

Mechanical strength and stretchability are important parameters of implants, influencing their handling during tendon surgery, which is often hampered by limited space at the operation site. High stretchability is particularly important because the tube has to be pulled over the sutured tendon and has to be enlarged transversally by forceps. Formation of fiber thickness, fiber orientation, and crosslinking, as well as nanotopographical structures like pores, ridges or grooves induce changes in the mechanical properties. Formation of such features is affected by many factors like polymer concentration and viscosity, applied voltage and flow rate, but also temperature and humidity during electrospinning [90]. Moreover, addition of substances, for instance proteins or platelet-rich plasma (PRP), influences mechanical properties showing reduced UTS with increased protein molecular weight [91] or formation of thicker fibers in the case of PRP [43]. However, fiber thickness is not the only parameter influencing mechanical strength as supplementation with HA/PEO in both ratios increased mechanical strength compared to pure DP scaffolds significantly while not influencing fiber thickness. Ultimate tensile stress of HA/PEO containing material was 2–3- times higher than in pure DP tubes, which was significantly different for axial and for transverse stretching, respectively. This is consistent with the data obtained by Chen et al. showing that addition of HA/iboprufen (IBU) increased mechanical properties of the scaffold without influencing fiber thickness [84]. Comparing the UTS of the same material, axial values were in general higher than transverse values most prominently pronounced in the 1:4 HA/PEO scaffold, which demonstrates the anisotropy of the scaffolds. Lower mechanical strength in the transverse direction might be a result of tertiary structures like ridges and grooves, acting as co-defects described by Evrova et al. [92]. As wall thickness has been shown to influence mechanical properties [43] the thinner wall diameter of the analyzed DP tubes (400 μm ± 57 μm), compared to the DP tubes used by Evrova et al. (500 − 800 μm) [92], might explain the slightly different results eventually caused by less pronounced formation of nanotopographic structures, such as grooves.

Pore size influences mechanical properties as well, depending on the scaffold material and the range of their size. For instance, in titanium scaffolds having pore sizes from 45 − 500 μm larger pore sizes reduced mechanical strength [93], while in hyaluronan/collagen scaffolds having pores ranging from 300 − 500 μm larger pores increased mechanical ultimate stresses and Young's Moduli [94]. Although pore size in the HA/PEO containing scaffolds was in average larger and mechanical properties were enhanced compared to pure DP scaffolds, influence of pore size on mechanical strength might nevertheless be irrelevant, as pores sizes were still quite similar in every material and the effect was probably rather caused by the chemical composition, *i.e.* addition of the HA/PEO layer. As for UTS, fracture strain of HA/PEO containing tubes showed 2- times higher values than DP tubes, which was a significant difference between the materials and found for axial and transverse stretching, demonstrating the great effect of a HA/PEO layer that influences mechanical strength and higher stretchability of the material. In addition, results from Young's modulus setting the UTS in relation to the length change were significantly lower for DP tubes compared with 1:4 ratio HA/PEO tubes but not compared with 1:1 ratio tubes, indicating the important role of PEO regarding mechanical scaffold properties. Polyethylene oxide, a non-toxic water-soluble synthetic polymer [95] improving electrospinning processability of aqueous solutions [83], has been shown to improve mechanical properties of commonly used biodegradable polymer electrospun scaffolds [96] and to result in increased UTS with increasing PEO concentrations [97]. The wetting of HA/PEO 1:1 bilayered scaffolds did not significantly influence UTS, fraction strain and Young's Moduli in the axial direction compared to dry material (Fig. S5). The relatively thin layer containing HA or the moderately hydrophobic material surface might be responsible that only little water was absorbed by the scaffold and therefore mechanical properties remained similar than before wetting.

In summary, addition of a HA/PEO layer increased the mechanical properties of DP scaffolds significantly, which facilitates the application of the implants during tendon surgery when material stretchability is needed mainly in the transverse direction; otherwise the tubular implant would break. However, it has to be emphasized that mechanical strength of the implants is too low to be used as reinforcement of injured tendons after surgery or in tendinopathy patients. For comparison, UTS of rabbit AT are in the range of 30 MPa and Young's modulus about 100 MPa [21] showing similar strength as human flexor tendons, while HA/PEO containing scaffolds showed for both, UTS and Young's modulus, *v*alues in the range of 1.5−2 MPa. However, as HA/PEO containing DP tubes are envisioned to reduce adhesion extent after surgery and not to act as tendon reinforcement, their low mechanical strength compared to native tendon tissue is not relevant for the envisioned application.

An important property of scaffolds used *in vitro* or *in vivo* is the wettability of the surface characterized by determination of the static water contact angle (WCA), influencing cellular attachment and proliferation as well as bacterial adhesion. Many factors are influencing the static WCA such as surface energy and roughness [72]. Surfaces with a static WCA lower than 90° are considered as hydrophilic, whereas hydrophobic surfaces show higher WCAs than 90°. Superhydrophobic materials with WCA between 150° and 180° have been shown to reduce bacterial adhesion and prevent biofilm formation [98]. Although HA and PEO are hydrophilic, static WCAs of HA/PEO containing scaffolds were only slightly lower than values from DP scaffolds and were not significantly different with values of about 100°. They were therefore classified as moderately hydrophobic materials (Fig. 2A). Another interesting characteristic is the difference between the advancing and the receding contact angle defined as CAH, which is attributed mainly to surface heterogeneity and roughness [69,71,72]. In the dynamic contact angle measurements, all different materials showed low receding angles, leading to a high hysteresis (Fig. 2A), indicating that scaffold surfaces are heterogeneous, which was confirmed by SEM images (Fig. 1). The roughness of the surfaces might explain the hydrophobic characteristics as contact angles can be increased with the surface roughness and air pockets at the water-scaffold interface [99].

Fourier-transform Infrared Spectroscopy was used to check possible changes in the transmission energy by the addition of HA and PEO, giving insights into the chemical composition of the tested materials (Fig. 2B). As expected, FTIR spectra of all tested scaffolds looked very similar because the amount of electrospun HA or PEO respectively, was very low (HA/PEO (1:1) about 5 % *w/v* each; HA/PEO (1:4) about 1.2 % w/v HA and 4.8 % w/v PEO) and therefore typical peaks of HA or PEO were superimposed by peaks of DP [50,73,86]. This result confirms data from Hu et al. showing that a low amount of supplemented substances does not change FTIR spectra [100]. However, when additional

bilayered patches were produced with an excessively thick HA/PEO layer and a very thin DP layer, the FTIR spectra clearly revealed the presence of HA/PEO. These materials were only produced to confirm HA/PEO, but were not used for *in vivo* experiments. The FTIR peaks were consistent with data from earlier DP measurements (Evrova, 2020); with a prominent peak at 1722 cm^{-1} assigned to the carbonyl group (C═O stretching) and a larger region at 1300–1000 $c\bar{m}^{1}$ associated with symmetric and asymmetric stretching vibrations of C—O junctions, both caused by ester bonds of the polyester urethane polymer DP [101,102]. Ratios of C═O bonds to C—O bonds were similar for all tested scaffolds (Fig. 2B) as described in chapter 3.3, unless the HA/PEO was used in excess compared to DP (Fig. 2B). In summary, the FTIR spectra indicate that no new bonds, between the DP polymer and HA or PEO respectively, were formed as peak pattern from pure DP scaffolds are identical to patterns of bilayered DP and HA/PEO scaffolds. The FTIR spectra of our implanted bilayered tubes (Fig. S2) suggest that relative amount of HA and PEO is small, and therefore these components were not detectable with FTIR.

To evaluate a possible change in thermal behavior by adding HA and PEO into electrospun DP scaffolds, the second DSC heating cycle was analyzed to determine the glass transition temperature (T_g), at which amorphous, solid material gets rubbery and viscous, and the melting point (T_m) of crystalline components [73] (Fig. 2C; for each single tube see Fig. S4). As expected, the additional HA/PEO layer did not change the typical thermal pattern of DP with a T_g at about −40 °C and a T_m at around 130 °C consistent with published data [58,86]. The prominent endothermic peak at about 56 °C corresponds to T_m of PEG or PEO, respectively. As PEO is used to enable proper HA electrospinning, it is present in the HA containing tubes, whereas the peak in the pure DP scaffolds results from incomplete washing of PEG that was used as first layer to facilitate taking off the tube from the metal rod [86]. Although the peak at 56 °C is smaller in pure DP scaffolds than in HA/PEO containing scaffolds and peak in HA/PEO scaffolds in a ratio 1:4 is slightly higher than in scaffolds with a ratio 1:1, it cannot be distinguished between PEG contamination and PEO integration in HA/PEO containing DP tubes. Interestingly, rests of PEG are detectable with DSC and also PEO contents might be seen in DSC thermograms, as corresponding peaks are moderately higher in DP/HA/PEO scaffolds.

SEM images showed that tenocytes were able to attach to the fibers of the different scaffold materials and immunocytochemical labeling for Collagen I, Fibronectin and α-SMA proofed that tenocytes were able to express ECM (Fig. 4). In general, stronger staining was observed for tenocytes seeded on HA/PEO in the ratio 1:1 than in the ratio 1:4, eventually due to the positive effect of HA on matrix organization, cell viability and cell activity [30,36]. In contrast to Fibronectin and α - SMA, less cells expressed Collagen I consistent with gene expression results from Miescher et al. [85], showing a decreased Collagen I expression in rabbit tenocytes using HMW HA (the same HA that was used here). Low Collagen I protein expression may further explain the anti-fibrotic, anti-adhesive effect observed during *in vivo* implantation. AlamarBlue™ assay confirmed attachment of tenocytes to scaffold fibers but showed reduced cell numbers over two weeks (Fig. S6), possibly due to limited permeability of nutrition, oxygen and metabolic waste within the scaffold [84] or due to the dense fiber network reducing proliferation and cell spreading [89].

The rabbit animal model has often been used to examine tendon healing and to enable translation of therapeutic assessments into clinical care [103]. For instance, cellular response towards DP implants [24], ultrasound studies [104] and adhesion formation [29,105] were studied using this model. The effect of HA/PEO containing DP tubes with a ratio 1:1 was evaluated regarding adhesion prevention in the rabbit full laceration AT model by histological analysis of the near contact region between the tendon and the surrounding tissue 3 weeks after surgery (Fig. 5). Results were compared with native tendons and with earlier results from repaired tendons with or without pure DP tube implantation [29]. Negligible adhesion towards the surrounding tissue was visible on Picrosirius Red and Hemalaun Sudan stained cross-sections of DP/HA/PEO tube-treated AT, comparable to native AT from the control contralateral legs (Fig. 5A), which was substantiated quantitatively (Fig. 5B). Impressively, while pure DP tubes decreased adhesion extent in 4-strand sutured tendons by about only 20 % in comparison with sutured tendons without tube [29], application of HA/PEO containing DP tube reduced adhesion significantly by about 50 % compared to sutured tendons treated with pure DP implants, reaching an adhesion extent similar to native tendons, *i.e.* negligible adhesions (Fig. 5B). Whether this convincing anti-adhesion effect was mechanistically provoked mainly by cell detachment from the scaffold upon PEO dissolution and/or by cells not at all adhering to it caused by the slippery surface of the lubricant HA, will remain open. Other reasons for this excellent anti-adhesive effects may be found in collagen I and other matrix proteins' downregulation of tendon cells in the vicinity of the implant, as *in vitro* results performed under stimulation with the same HMW HA have shown before [54]. However, anti-adhesive effects of HA could be observed not only towards the surrounding tissue, but also towards the tendon tissue. This side effect may be caused by HA diffusion and the strong lubricating properties of HA even in small amounts also on the side of the pure DP layer. The unexpected anti-adhesive effect towards the tendon might be reduced by a further DP layer with incorporated growth factors for better attachment to the repaired tendon and prevention of HA diffusion to this site [86], and additionally enhancing tendon regeneration as has been previously shown by Evrova et al. [58].

As with every work, there are some limitations. We did not systematically investigate if cell attachment was different on fibers of smooth or rough surfaces of the same electrospun material as cell attachment and growth are due to the purpose of the implant to reduce adhesion formation not the main focus of the study. Finally, we selected three types of extracellular matrix proteins to check ECM expression of rabbit Achilles tenocytes seeded on the different materials, where other markers, such as Collagen III protein expression would also be interesting. Finally, we did our rabbit experiments only until 3 weeks post-surgery, however, longer time points post-operation might be interesting to be checked for adhesion extent as well.

5. Conclusion

We have produced a novel electrospun implant with a pure DP layer and a second layer of HA/PEO with the aim to reduce adhesion formation in a rabbit full laceration Achilles tendon model even more than by the pure DP implant (20 % reduction). The results from the 3-week *in vivo* assessment demonstrate that adhesion extent was reduced significantly by around 50 % compared to a pure DP implant, reaching a level comparable to healthy tendons. *In vitro* studies have shown that rabbit tenocytes were able to attach on every scaffold material, but cell numbers decreased over a time period of 2 weeks, probably due to the limited permeability for nutrition, oxygen and metabolic waste within the scaffold or due to the dense fiber network sensed by the tenocytes and reducing proliferation in consequence. The novel scaffolds were characterized in detail, including fiber thickness that was for all scaffolds in the range of 5–10 μm and pore size (SEM) which was in the range of 5–10 μm for HA/PEO and $<$ 5 μm for pure DP fiber meshes; FTIR which confirmed both materials in the electrospun meshes by according peak wavenumbers; DSC that revealed T_g at −40 °C, T_m at 130 °C and a peak for PEG or PEO, respectively, at 56 °C; static and dynamic WCA and mechanical tests that substantiated the positive impact of the HA/PEO layer when compared to pure DP. This study demonstrates that an additional HA/PEO layer on an electrospun DP scaffold shows promising potential in reducing adhesion formation after tendon surgery. Therefore, these novel bilayered implants show great potential for a clinical application in the future.

CRediT authorship contribution statement

Conceptualization, I.M., J.B.; methodology, I.M., E.O., A.M. and Y.Y.; software, I.M.; validation, I.M. and E.O.; formal analysis, I.M., investigation, I.M., N.C., G.M.B., J.R., Y.Y., A.M., E.O. and M.C.; resources, J.B.; data curation, I.M. and E.O.; writing—original draft preparation, I.M. and J.B.; writing—review and editing, I.M. and J.B.; visualization, I.M. and J.B.; supervision, I.M., J.G.S., V.V. and J.B.; project administration, J.B.; funding acquisition, J.B. All authors have read and agreed to the published version of the manuscript.

Funding

This research was funded by the *Swiss National Science Foundation SNSF*, grant number 310030_197578.

Institutional review board statement

Not applicable.

Informed consent statement

Not applicable.

Declaration of competing interest

The authors declare that they do not have any competing interests.

Data availability

Data will be made available on request.

Acknowledgments

We are very much indebted for financial support by the Swiss National Science Foundation SNSF (grant number 310030_197578). We thank Ab Medica, Italy, for providing DegraPol® polymer. Flora Nicholls is highly acknowledged for her help with rabbit Achilles tendons for the isolation of tenocytes. We thank Ines Kleiber-Schaaf and Andrea Garcete-Bärtschi for the preparation of the scaffold slides and immunocytochemical staining. The authors acknowledge the assistance and support of the Center for Microscopy and Image Analysis (ZMB), University of Zurich, for performing scanning electron microscopy (SEM). Furthermore, we highly acknowledge the fact that we were allowed to use the FTIR facility of Prof. Raffaele Mezzenga's laboratory at ETH Zurich. The help of Dr. Kirill Feldman with regard to DSC measurements is highly acknowledged. Finally, we highly acknowledge Dr. Minghan Hu and Prof. Lucio Isa for access to their water contact angle machine in the laboratory of Soft Materials and Interfaces at ETH Zurich.

Appendix A. Supplementary data

Supplementary data to this article can be found online at https://doi.org/10.1016/j.ijbiomac.2024.133193.

References

[1] J.B. Tang, Basic FGF or VEGF gene therapy corrects insufficiency in the intrinsic healing capacity of tendons, Sci. Rep. 6 (2016), https://doi.org/10.1038/srep20643.
[2] S.W. Linderman, R.H. Gelberman, S. Thomopoulos, H. Shen, Cell and biologic-based treatment of flexor tendon injuries, Oper. Tech. Orthop. 26 (2016) 206–215, https://doi.org/10.1053/j.oto.2016.06.011.
[3] L.M. Galatz, L. Gerstenfeld, E. Heber-Katz, S.A. Rodeo, Tendon regeneration and scar formation: the concept of scarless healing, J. Orthop. Res. 33 (2015) 823–831, https://doi.org/10.1002/jor.22853.
[4] J.E. Gaida, J.L. Cook, S.L. Bass, Adiposity and tendinopathy, Disabil. Rehabil. 30 (2008) 1555–1562, https://doi.org/10.1080/09638280701786864.
[5] R.A. Clayton, C.M. Court-Brown, The epidemiology of musculoskeletal tendinous and ligamentous injuries, Injury 39 (2008) 1338–1344, https://doi.org/10.1016/j.injury.2008.06.021.
[6] J.P. de Jong, J.T. Nguyen, A.J. Sonnema, E.C. Nguyen, P.C. Amadio, S.L. Moran, The incidence of acute traumatic tendon injuries in the hand and wrist: a 10-year population-based study, Clin. Orthop. Surg. 6 (2014) 196–202, https://doi.org/10.4055/cios.2014.6.2.196.
[7] Z. Ren, Z. Duan, Z. Zhang, R. Fu, C. Zhu, D. Fan, Instantaneous self-healing and strongly adhesive self-adaptive hyaluronic acid-based hydrogel for controlled drug release to promote tendon wound healing, Int. J. Biol. Macromol. 242 (2023) 125001, https://doi.org/10.1016/j.ijbiomac.2023.125001.
[8] J.G. Graham, M.L. Wang, M. Rivlin, P.K. Beredjiklian, Biologic and mechanical aspects of tendon fibrosis after injury and repair, Connect. Tissue Res. 60 (2019) 10–20, https://doi.org/10.1080/03008207.2018.1512979.
[9] P. Sharma; N. Maffulli. Biology of tendon injury: healing, modeling and remodeling. J. Musculoskelet. Neuronal Interact. 6 (2006) 181–190. Retrieved from **https://www.ismni.org/jmni/index.php**.
[10] P.B. Voleti, M.R. Buckley, L.J. Soslowsky, Tendon healing: repair and regeneration, Annu. Rev. Biomed. Eng. 14 (2012) 47–71, https://doi.org/10.1146/annurev-bioeng-071811-150122.
[11] A.L. Titan, D.S. Foster, J. Chang, M.T. Longaker, Flexor tendon: development, healing, adhesion formation, and contributing growth factors, Plast. Reconstr. Surg. 144 (2019) 639e–647e, https://doi.org/10.1097/prs.0000000000006048.
[12] N. Juncosa-Melvin, J.T. Shearn, G.P. Boivin, C. Gooch, M.T. Galloway, J.R. West, V.S. Nirmalanandhan, G. Bradica, D.L. Butler, Effects of mechanical stimulation on the biomechanics and histology of stem cell-collagen sponge constructs for rabbit patellar tendon repair, Tissue Eng. 12 (2006) 2291–2300, https://doi.org/10.1089/ten.2006.12.2291.
[13] G. Walden, X. Liao, S. Donell, M.J. Raxworthy, G.P. Riley, A. Saeed, A clinical, biological, and biomaterials perspective into tendon injuries and regeneration, Tissue Eng. Part B Rev. 23 (2017) 44–58, https://doi.org/10.1089/ten.TEB.2016.0181.
[14] A.E. Loiselle, G.A. Bragdon, J.A. Jacobson, S. Hasslund, Z.E. Cortes, E. M. Schwarz, D.J. Mitten, H.A. Awad, R.J. O'Keefe, Remodeling of murine intrasynovial tendon adhesions following injury: MMP and neotendon gene expression, J. Orthop. Res. 27 (2009) 833–840, https://doi.org/10.1002/jor.20769.
[15] C.S. Proctor, D.W. Jackson, T.M. Simon, Characterization of the repair tissue after removal of the central one-third of the patellar ligament. An experimental study in a goat model, J. Bone Joint Surg. Am. 79 (1997) 997–1006, https://doi.org/10.2106/00004623-199707000-00005.
[16] J.E. Carpenter, S. Thomopoulos, C.L. Flanagan, C.M. DeBano, L.J. Soslowsky, Rotator cuff defect healing: a biomechanical and histologic analysis in an animal model, J. Shoulder Elb. Surg. 7 (1998) 599–605, https://doi.org/10.1016/s1058-2746(98)90007-6.
[17] J.B. Tang, Clinical outcomes associated with flexor tendon repair, Hand Clin. 21 (2005) 199–210, https://doi.org/10.1016/j.hcl.2004.11.005.
[18] F. Veronesi, G. Giavaresi, D. Bellini, V. Casagranda, D. Pressato, M. Fini, Evaluation of a new collagen-based medical device (ElastiCo®) for the treatment of acute Achilles tendon injury and prevention of peritendinous adhesions: an in vitro biocompatibility and in vivo investigation, J. Tissue Eng. Regen. Med. 14 (2020) 1113–1125, https://doi.org/10.1002/term.3085.
[19] H.J. Goodman, J. Choueka, Biomechanics of the flexor tendons, Hand Clin. 21 (2005) 129–149, https://doi.org/10.1016/j.hcl.2004.11.002.
[20] G. Meier Bürgisser, M. Calcagni, E. Bachmann, G. Fessel, J.G. Snedeker, P. Giovanoli, J. Buschmann, Rabbit Achilles tendon full transection model - wound healing, adhesion formation and biomechanics at 3, 6 and 12 weeks post-surgery, Biol Open 5 (2016) 1324–1333, https://doi.org/10.1242/bio.020644.
[21] G. Meier Bürgisser; M. Calcagni; A. Müller; E. Bonavoglia; G. Fessel; J.G. Snedeker; P. Giovanoli; J. Buschmann. Prevention of peritendinous adhesions using an electrospun DegraPol polymer tube: a histological, ultrasonographic, and biomechanical study in rabbits. Biomed. Res. Int. 2014 (2014) 656240. **doi:** https://doi.org/10.1155/2014/656240.
[22] C. Chartier, H. ElHawary, A. Baradaran, J. Vorstenbosch, L. Xu, J.I. Efanov, Tendon: principles of healing and repair, Semin. Plast. Surg. 35 (2021) 211–215, https://doi.org/10.1055/s-0041-1731632.
[23] H. Zhao, H.G. Guan, J. Gu, Z.P. Luo, W. Zhang, B. Chen, Q.L. Gu, H.L. Yang, Q. Shi, Collagen membrane alleviates peritendinous adhesion in the rat Achilles tendon injury model, Chin. Med. J. 126 (2013) 729–733, https://doi.org/10.3760/cma.j.issn.0366-6999.20122566.
[24] J. Buschmann, M. Calcagni, G.M. Bürgisser, E. Bonavoglia, P. Neuenschwander, V. Milleret, P. Giovanoli, Synthesis, characterization and histomorphometric analysis of cellular response to a new elastic DegraPol® polymer for rabbit Achilles tendon rupture repair, J. Tissue Eng. Regen. Med. 9 (2015) 584–594, https://doi.org/10.1002/term.1624.
[25] E. Chen, L. Yang, C. Ye, W. Zhang, J. Ran, D. Xue, Z. Wang, Z. Pan, Q. Hu, An asymmetric chitosan scaffold for tendon tissue engineering: in vitro and in vivo evaluation with rat tendon stem/progenitor cells, Acta Biomater. 73 (2018) 377–387, https://doi.org/10.1016/j.actbio.2018.04.027.
[26] M. Lipar, B. Zdilar, M. Kreszinger, M. Ćorić, B. Radišić, M. Samardžija, R. Žic, M. Pećin, Extracellular matrix supports healing of transected rabbit Achilles tendon, Heliyon 4 (2018) e00781, https://doi.org/10.1016/j.heliyon.2018.e00781.
[27] B. Saad, O.M. Keiser, M. Welti, G.K. Uhlschmid, P. Neuenschwander, U.W. Suter, Multiblock copolyesters as biomaterials: in vitro biocompatibility testing,

J. Mater. Sci. Mater. Med. 8 (1997) 497–505, https://doi.org/10.1023/a:1018582311361.
[28] J. Buschmann, G. Meier-Bürgisser, E. Bonavoglia, P. Neuenschwander, V. Milleret, P. Giovanoli, M. Calcagni, Cellular response of healing tissue to DegraPol tube implantation in rabbit Achilles tendon rupture repair: an in vivo histomorphometric study, J. Tissue Eng. Regen. Med. 7 (2013) 413–420, https://doi.org/10.1002/term.538.
[29] G.M. Bürgisser, O. Evrova, D.M. Heuberger, P. Wolint, J. Rieber, I. Miescher, R. A. Schüpbach, P. Giovanoli, M. Calcagni, J. Buschmann, Electrospun tube reduces adhesion in rabbit Achilles tendon 12 weeks post-surgery without PAR-2 overexpression, Sci. Rep. 11 (2021) 23293, https://doi.org/10.1038/s41598-021-02780-4.
[30] A. Fallacara, E. Baldini, S. Manfredini, S. Vertuani, Hyaluronic acid in the third millennium, Polymers 10 (2018), https://doi.org/10.3390/polym10070701.
[31] T. Kobayashi, T. Chanmee, N. Itano, Hyaluronan: metabolism and function, Biomolecules 10 (2020), https://doi.org/10.3390/biom10111525.
[32] M. Abate, C. Schiavone, V. Salini, The use of hyaluronic acid after tendon surgery and in tendinopathies, Biomed. Res. Int. 2014 (2014) 783632, https://doi.org/10.1155/2014/783632.
[33] D. Tercic, B. Bozic, The basis of the synovial fluid analysis, Clin. Chem. Lab. Med. 39 (2001) 1221–1226, https://doi.org/10.1515/cclm.2001.196.
[34] E.A. Balazs, D. Watson, I.F. Duff, S. Roseman, Hyaluronic acid in synovial fluid. I. Molecular parameters of hyaluronic acid in normal and arthritis human fluids, Arthritis Rheum. 10 (1967) 357–376, https://doi.org/10.1002/art.1780100407.
[35] K.L. Aya, R. Stern, Hyaluronan in wound healing: rediscovering a major player, Wound Repair Regen. 22 (2014) 579–593, https://doi.org/10.1111/wrr.12214.
[36] L. Osti, M. Berardocco, V. di Giacomo, G. Di Bernardo, F. Oliva, A.C. Berardi, Hyaluronic acid increases tendon derived cell viability and collagen type I expression in vitro: comparative study of four different hyaluronic acid preparations by molecular weight, BMC Musculoskelet. Disord. 16 (2015) 284, https://doi.org/10.1186/s12891-015-0735-7.
[37] H. Li, Y. Chen, S. Chen, Enhancement of rotator cuff tendon-bone healing using bone marrow-stimulating technique along with hyaluronic acid, Journal of orthopaedic translation 17 (2019) 96–102, https://doi.org/10.1016/j.jot.2019.01.001.
[38] J.F. Kaux, A. Samson, J.M. Crielaard, Hyaluronic acid and tendon lesions, Muscles, ligaments and tendons journal 5 (2015) 264–269, https://doi.org/10.11138/mltj/2015.5.4.264.
[39] C. Loebel, T. Stauber, M. D'Este, M. Alini, M. Zenobi-Wong, D. Eglin, Fabrication of cell-compatible hyaluronan hydrogels with a wide range of biophysical properties through high tyramine functionalization, J. Mater. Chem. B 5 (2017) 2355–2363, https://doi.org/10.1039/c6tb03161g.
[40] H. Honda, M. Gotoh, T. Kanazawa, H. Ohzono, H. Nakamura, K. Ohta, K. I. Nakamura, K. Fukuda, T. Teramura, T. Hashimoto, et al., Hyaluronic acid accelerates tendon-to-bone healing after rotator cuff repair, Am. J. Sports Med. 45 (2017) 3322–3330, https://doi.org/10.1177/0363546517720199.
[41] J.I. Liang, P.C. Lin, M.Y. Chen, T.H. Hsieh, J.J. Chen, M.L. Yeh, The effect of tenocyte/hyaluronic acid therapy on the early recovery of healing Achilles tendon in rats, J. Mater. Sci. Mater. Med. 25 (2014) 217–227, https://doi.org/10.1007/s10856-013-5036-9.
[42] E. Murray, D. Challoumas, A. Putti, N. Millar, Effectiveness of sodium hyaluronate and ADCON-T/N for the prevention of adhesions in hand flexor tendon surgery: a systematic review and Meta-analysis, J. Hand. Surg. [Am.] 47 (896) (2022) e891–896.e820, https://doi.org/10.1016/j.jhsa.2021.07.012.
[43] C.H. Chen, S.H. Chen, S.H. Chen, A.D. Chuang, G.D. T; J.P. Chen., Hyaluronic acid/platelet rich plasma-infused core-shell nanofiber membrane to prevent postoperative tendon adhesion and promote tendon healing, Int. J. Biol. Macromol. 231 (2023) 123312, https://doi.org/10.1016/j.ijbiomac.2023.123312.
[44] E.R. McDermott, Z. Bowers, J.A. Nuelle, The application of hyaluronic acid/alginate sheet to flexor Pollicis longus tendon repair to prevent adhesion formation: a second look, Cureus 14 (2022) e33147, https://doi.org/10.7759/cureus.33147.
[45] K.C. Castro, M.G.N. Campos, L.H.I. Mei, Hyaluronic acid electrospinning: challenges, applications in wound dressings and new perspectives, Int. J. Biol. Macromol. 173 (2021) 251–266, https://doi.org/10.1016/j.ijbiomac.2021.01.100.
[46] J.E. Rayahin, J.S. Buhrman, Y. Zhang, T.J. Koh, R.A. Gemeinhart, High and low molecular weight hyaluronic acid differentially influence macrophage activation, ACS Biomater Sci. Eng. 1 (2015) 481–493, https://doi.org/10.1021/acsbiomaterials.5b00181.
[47] V. Vassallo, A. Stellavato, D. Cimini, A.V.A. Pirozzi, A. Alfano, M. Cammarota, G. Balato, A. D'Addona, C. Ruosi, C. Schiraldi, Unsulfated biotechnological chondroitin by itself as well as in combination with high molecular weight hyaluronan improves the inflammation profile in osteoarthritis in vitro model, J. Cell. Biochem. 122 (2021) 1021–1036, https://doi.org/10.1002/jcb.29907.
[48] A. D'Agostino, A. Stellavato, L. Corsuto, P. Diana, R. Filosa, A. La Gatta, M. De Rosa, C. Schiraldi, Is molecular size a discriminating factor in hyaluronan interaction with human cells? Carbohydr. Polym. 157 (2017) 21–30, https://doi.org/10.1016/j.carbpol.2016.07.125.
[49] Y. Gao, Y. Sun, H. Yang, P. Qiu, Z. Cong, Y. Zou, L. Song, J. Guo, T. P. Anastassiades, A low molecular weight hyaluronic acid derivative accelerates excisional wound healing by modulating pro-inflammation, promoting epithelialization and neovascularization, and remodeling collagen, Int. J. Mol. Sci. 20 (2019), https://doi.org/10.3390/ijms20153722.
[50] A. Chanda, J. Adhikari, A. Ghosh, S.R. Chowdhury, S. Thomas, P. Datta, P. Saha, Electrospun chitosan/polycaprolactone-hyaluronic acid bilayered scaffold for potential wound healing applications, Int. J. Biol. Macromol. 116 (2018) 774–785, https://doi.org/10.1016/j.ijbiomac.2018.05.099.
[51] F.E. Karabekmez, C. Zhao, Surface treatment of flexor tendon autograft and allograft decreases adhesion without an effect of graft cellularity: a pilot study, Clin. Orthop. Relat. Res. 470 (2012) 2522–2527, https://doi.org/10.1007/s11999-012-2437-x.
[52] L.A. Smith, P.X. Ma, Nano-fibrous scaffolds for tissue engineering, Colloids Surf. B: Biointerfaces 39 (2004) 125–131, https://doi.org/10.1016/j.colsurfb.2003.12.004.
[53] D.R. Figueira, S.P. Miguel, K.D. de Sá, I.J. Correia, Production and characterization of polycaprolactone- hyaluronic acid/chitosan- zein electrospun bilayer nanofibrous membrane for tissue regeneration, Int. J. Biol. Macromol. 93 (2016) 1100–1110, https://doi.org/10.1016/j.ijbiomac.2016.09.080.
[54] I. Miescher, P. Wolint, C. Opelz, J.G. Snedeker, P. Giovanoli, M. Calcagni, J. Buschmann, Impact of high-molecular-weight hyaluronic acid on gene expression in rabbit Achilles tenocytes in vitro, Int. J. Mol. Sci. 23 (2022) 7926, https://doi.org/10.3390/ijms23147926.
[55] R.K. Reed, U.B. Laurent, J.R. Fraser, T.C. Laurent, Removal rate of [3H] hyaluronan injected subcutaneously in rabbits, Am. J. Phys. 259 (1990) H532–H535, https://doi.org/10.1152/ajpheart.1990.259.2.H532.
[56] P. Snetkov, S. Morozkina, M. Uspenskaya, R. Olekhnovich, Hyaluronan-based nanofibers: fabrication, Characterization and Application. Polymers (Basel) 11 (2019), https://doi.org/10.3390/polym11122036.
[57] A. Memic, T. Abudula, H.S. Mohammed, K. Joshi Navare, T. Colombani, S. A. Bencherif, Latest Progress in electrospun nanofibers for wound healing applications, ACS Appl. Bio Mater. 2 (2019) 952–969, https://doi.org/10.1021/acsabm.8b00637.
[58] O. Evrova, G.M. Bürgisser, C. Ebnöther, A. Adathala, M. Calcagni, E. Bachmann, J.G. Snedeker, C. Scalera, P. Giovanoli, V. Vogel, J. Buschmann, Elastic and surgeon friendly electrospun tubes delivering PDGF-BB positively impact tendon rupture healing in a rabbit Achilles tendon model, Biomaterials 232 (2020) 119722, https://doi.org/10.1016/j.biomaterials.2019.119722.
[59] J. Buschmann, A. Müller, K. Feldman, T.A. Tervoort, G. Fessel, J.G. Snedeker, P. Giovanoli, M. Calcagni, Small hook thread (Quill) and soft felt internal splint to increase the primary repair strength of lacerated rabbit Achilles tendons: biomechanical analysis and considerations for hand surgery, Clin. Biomech. (Bristol, Avon) 26 (2011) 626–631, https://doi.org/10.1016/j.clinbiomech.2011.02.003.
[60] D. Docheva, S.A. Müller, M. Majewski, C.H. Evans, Biologics for tendon repair, Adv. Drug Deliv. Rev. 84 (2015) 222–239, https://doi.org/10.1016/j.addr.2014.11.015.
[61] N.L. Leong, J.L. Kator, T.L. Clemens, A. James, M. Enamoto-Iwamoto, J. Jiang, Tendon and ligament healing and current approaches to tendon and ligament regeneration, J. Orthop. Res. 38 (2020) 7–12, https://doi.org/10.1002/jor.24475.
[62] L. Vítková, L. Musilová, E. Achbergerová, A. Minařík, P. Smolka, E. Wrzecionko, A. Mráček, Electrospinning of Hyaluronan using polymer Coelectrospinning and intermediate solvent, Polymers 11 (2019), https://doi.org/10.3390/polym11091517.
[63] F. Bassetto, G. Pajardi, B. Battiston, M. Corain, S. Sargenti, C. Scarpa, C. Novelli, C. Tiengo, A. Vitali, F. Facchin, et al., Efficacy and safety of Dynavisc® gel in prevention of scar adhesions recurrence after flexor tendons tenolysis in zone 2. Multicenter retrospective cohort study, Ann. Ital. Chir. 94 (2023) 529–536. Retrieved from, **https://annaliitalianidichirurgia.it**.
[64] K. Shameli, M. Bin Ahmad, S.D. Jazayeri, S. Sedaghat, P. Shabanzadeh, H. Jahangirian, M. Mahdavi, Y. Abdollahi, Synthesis and characterization of polyethylene glycol mediated silver nanoparticles by the green method, Int. J. Mol. Sci. 13 (2012) 6639–6650, https://doi.org/10.3390/ijms13066639.
[65] M. Rozenberg, A. Loewenschuss, Y. Marcus, IR spectra and hydration of short-chain polyethyleneglycols, Spectrochim. Acta A Mol. Biomol. Spectrosc. 54 (1998) 1819–1826, https://doi.org/10.1016/S1386-1425(98)00062-6.
[66] N. Vahedi, F. Tabandeh, M. Mahmoudifard, Hyaluronic acid-graphene quantum dot nanocomposite: potential target drug delivery and cancer cell imaging, Biotechnol. Appl. Biochem. 69 (2022) 1068–1079, https://doi.org/10.1002/bab.2178.
[67] L.O. Alcântara, J.R. de Sousa, F.K. Andrade, E.H. Teixeira, M. Cerqueira, A.L.C. da Silva, M.S.M. Souza Filho, B.W.S. de Souza, Extraction and characterization of hyaluronic acid from the eyeball of Nile Tilapia (Oreochromis niloticus), Int. J. Biol. Macromol. 226 (2023) 172–183, https://doi.org/10.1016/j.ijbiomac.2022.12.016.
[68] M. Hu, K. Korschelt, M. Viel, N. Wiesmann, M. Kappl, J. Brieger, K. Landfester, H. Thérien-Aubin, W. Tremel, Nanozymes in Nanofibrous Mats with Haloperoxidase-like activity to combat biofouling, ACS Appl. Mater. Interfaces 10 (2018) 44722–44730, https://doi.org/10.1021/acsami.8b16307.
[69] H.B. Eral, 't Mannetje, D.J.C.M., and Oh, J.M., Contact angle hysteresis: a review of fundamentals and applications, Colloid Polym. Sci. 291 (2) (2013) 247–260, https://doi.org/10.1007/s00396-012-2796-6.
[70] O. Evrova, D. Kellenberger, M. Calcagni, V. Vogel, J. Buschmann, Supporting cell-based tendon therapy: effect of PDGF-BB and ascorbic acid on rabbit Achilles tenocytes in vitro, Int. J. Mol. Sci. 21 (2020), https://doi.org/10.3390/ijms21020458.
[71] C.W. Extrand, Y. Kumagai, An experimental study of contact angle hysteresis, J. Colloid Interface Sci. 191 (1997) 378–383, https://doi.org/10.1006/jcis.1997.4935.

[72] B.B.Y.C. Jung, Contact angle, adhesion and friction properties of micro- and nanopatterned polymers for superhydrophobicity, Nanotechnology 17 (2006) 4970–4980, https://doi.org/10.1088/0957-4484/17/19/033.
[73] K.T. Shalumon, C. Sheu, C.H. Chen, S.H. Chen, G. Jose, C.Y. Kuo, J.P. Chen, Multi-functional electrospun antibacterial core-shell nanofibrous membranes for prolonged prevention of post-surgical tendon adhesion and inflammation, Acta Biomater. 72 (2018) 121–136, https://doi.org/10.1016/j.actbio.2018.03.044.
[74] G.G. Schulze-Tanzil, M. Delgado-Calcares, R. Stange, B. Wildemann, D. Docheva, Tendon healing: a concise review on cellular and molecular mechanisms with a particular focus on the Achilles tendon, Bone Joint Res 11 (2022) 561–574, https://doi.org/10.1302/2046-3758.118.Bjr-2021-0576.R1.
[75] S.G. Parekh, F.S. Aran, S. Mithani, A. Chopra, Achilles: failed acute repair, Foot Ankle Clin. 27 (2022) 415–430, https://doi.org/10.1016/j.fcl.2021.11.026.
[76] S. Chen, S. Jiang, W. Zheng, B. Tu, S. Liu, H. Ruan, C. Fan, RelA/p65 inhibition prevents tendon adhesion by modulating inflammation, cell proliferation, and apoptosis, Cell Death Dis. 8 (2017) e2710, https://doi.org/10.1038/cddis.2017.135.
[77] S.H. Taylor, S. Al-Youha, T. Van Agtmael, Y. Lu, J. Wong, D.A. McGrouther, K. E. Kadler, Tendon is covered by a basement membrane epithelium that is required for cell retention and the prevention of adhesion formation, PLoS One 6 (2011) e16337, https://doi.org/10.1371/journal.pone.0016337.
[78] D. Elliot, T. Giesen, Primary flexor tendon surgery: the search for a perfect result, Hand Clin. 29 (2013) 191–206, https://doi.org/10.1016/j.hcl.2013.03.001.
[79] A. Imere, C. Ligorio, M. O'Brien, J.K.F. Wong, M. Domingos, S.H. Cartmell, Engineering a cell-hydrogel-fibre composite to mimic the structure and function of the tendon synovial sheath, Acta Biomater. 119 (2021) 140–154, https://doi.org/10.1016/j.actbio.2020.11.017.
[80] F. Oliva, E. Marsilio, G. Asparago, A. Frizziero, A.C. Berardi, N. Maffulli, The impact of hyaluronic acid on tendon physiology and its clinical application in tendinopathies, Cells 10 (2021), https://doi.org/10.3390/cells10113081.
[81] M. Marian, R. Shah, B. Gashi, S. Zhang, K. Bhavnani, S. Wartzack, A. Rosenkranz, Exploring the lubrication mechanisms of synovial fluids for joint longevity - a perspective, Colloids Surf. B: Biointerfaces 206 (2021) 111926, https://doi.org/10.1016/j.colsurfb.2021.111926.
[82] N. Pien, I. Peeters, L. Deconinck, L. Van Damme, L. De Wilde, A. Martens, S. Van Vlierberghe, P. Dubruel, A. Mignon, Design and development of a reinforced tubular electrospun construct for the repair of ruptures of deep flexor tendons, Mater. Sci. Eng. C Mater. Biol. Appl. 119 (2021) 111504, https://doi.org/10.1016/j.msec.2020.111504.
[83] C. Yao, X. Li, T. Song, Fabrication of zein/hyaluronic acid fibrous membranes by electrospinning, J. Biomater. Sci. Polym. Ed. 18 (2007) 731–742, https://doi.org/10.1163/156856207781034070.
[84] C.T. Chen, C.H. Chen, C. Sheu, J.P. Chen, Ibuprofen-loaded hyaluronic acid Nanofibrous membranes for prevention of postoperative tendon adhesion through reduction of inflammation, Int. J. Mol. Sci. 20 (2019), https://doi.org/10.3390/ijms20205038.
[85] I. Miescher, P. Wolint, C. Opelz, J.G. Snedeker, P. Giovanoli, M. Calcagni, J. Buschmann, Impact of high-molecular-weight hyaluronic acid on gene expression in rabbit Achilles tenocytes in vitro, Int. J. Mol. Sci. 23 (2022), https://doi.org/10.3390/ijms23147926.
[86] J. Rieber, G. Meier-Bürgisser, I. Miescher, F.E. Weber, P. Wolint, Y. Yao, E. Ongini, A. Milionis, J.G. Snedeker, M. Calcagni, J. Buschmann, Bioactive and elastic emulsion electrospun DegraPol tubes delivering IGF-1 for tendon rupture repair, Int. J. Mol. Sci. 24 (2023), https://doi.org/10.3390/ijms241210272.
[87] O. Evrova, J. Houska, M. Welti, E. Bonavoglia, M. Calcagni, P. Giovanoli, V. Vogel, J. Buschmann, Bioactive, elastic, and biodegradable emulsion electrospun DegraPol tube delivering PDGF-BB for tendon rupture repair, Macromol. Biosci. 16 (2016) 1048–1063, https://doi.org/10.1002/mabi.201500455.
[88] Y. Chen, G.Z. Tan, Y. Zhou, Effects of viscosities and solution composition on Core-sheath electrospun Polycaprolactone(PCL) Nanoporous microtubes, Polymers 13 (2021), https://doi.org/10.3390/polym13213650.
[89] B.M. Baker, B. Trappmann, W.Y. Wang, M.S. Sakar, I.L. Kim, V.B. Shenoy, J. A. Burdick, C.S. Chen, Cell-mediated fibre recruitment drives extracellular matrix mechanosensing in engineered fibrillar microenvironments, Nat. Mater. 14 (2015) 1262–1268, https://doi.org/10.1038/nmat4444.
[90] S.G. Kumbar, R. James, S.P. Nukavarapu, C.T. Laurencin, Electrospun nanofiber scaffolds: engineering soft tissues, Biomed. Mater. 3 (2008) 034002, https://doi.org/10.1088/1748-6041/3/3/034002.
[91] D.M. Lavin, L. Zhang, S. Furtado, R.A. Hopkins, E. Mathiowitz, Effects of protein molecular weight on the intrinsic material properties and release kinetics of wet spun polymeric microfiber delivery systems, Acta Biomater. 9 (2013) 4569–4578, https://doi.org/10.1016/j.actbio.2012.08.005.
[92] O. Evrova, J. Houska, M. Welti, E. Bonavoglia, M. Calcagni, P. Giovanoli, V. Vogel, J. Buschmann, Bioactive, elastic, and biodegradable emulsion electrospun DegraPol tube delivering PDGF-BB for tendon rupture repair, Macromol. Biosci. 16 (2016) 1048–1063, https://doi.org/10.1002/mabi.201500455.
[93] C. Torres-Sanchez, F.R.A. Al Mushref, M. Norrito, K. Yendall, Y. Liu, P.P. Conway, The effect of pore size and porosity on mechanical properties and biological response of porous titanium scaffolds, Mater. Sci. Eng. C Mater. Biol. Appl. 77 (2017) 219–228, https://doi.org/10.1016/j.msec.2017.03.249.
[94] A.A. Al-Munajjed, M. Hien, R. Kujat, J.P. Gleeson, J. Hammer, Influence of pore size on tensile strength, permeability and porosity of hyaluronan-collagen scaffolds, J. Mater. Sci. Mater. Med. 19 (2008) 2859–2864, https://doi.org/10.1007/s10856-008-3422-5.
[95] B.M. Baker, A.O. Gee, R.B. Metter, A.S. Nathan, R.A. Marklein, J.A. Burdick, R. L. Mauck, The potential to improve cell infiltration in composite fiber-aligned electrospun scaffolds by the selective removal of sacrificial fibers, Biomaterials 29 (2008) 2348–2358, https://doi.org/10.1016/j.biomaterials.2008.01.032.
[96] J. Hodge, C. Quint, The improvement of cell infiltration in an electrospun scaffold with multiple synthetic biodegradable polymers using sacrificial PEO microparticles, J. Biomed. Mater. Res. A 107 (2019) 1954–1964, https://doi.org/10.1002/jbm.a.36706.
[97] R. Serôdio, S.L. Schickert, A.R. Costa-Pinto, J.R. Dias, P.L. Granja, F. Yang, A. L. Oliveira, Ultrasound sonication prior to electrospinning tailors silk fibroin/PEO membranes for periodontal regeneration, Mater. Sci. Eng. C Mater. Biol. Appl. 98 (2019) 969–981, https://doi.org/10.1016/j.msec.2019.01.055.
[98] K. Bartlet, S. Movafaghi, L.P. Dasi, A.K. Kota, K.C. Popat, Antibacterial activity on superhydrophobic titania nanotube arrays, Colloids Surf. B: Biointerfaces 166 (2018) 179–186, https://doi.org/10.1016/j.colsurfb.2018.03.019.
[99] A. Salam, M.Q. Khan, T. Hassan, N. Hassan, A. Nazir, T. Hussain, M. Azeem, I. S. Kim, In-vitro assessment of appropriate hydrophilic scaffolds by co-electrospinning of poly(1,4 cyclohexane isosorbide terephthalate)/polyvinyl alcohol, Sci. Rep. 10 (2020) 19751, https://doi.org/10.1038/s41598-020-76471-x.
[100] J. Hu, M.P. Prabhakaran, X. Ding, S. Ramakrishna, Emulsion electrospinning of polycaprolactone: influence of surfactant type towards the scaffold properties, J. Biomater. Sci. Polym. Ed. 26 (2015) 57–75, https://doi.org/10.1080/09205063.2014.982241.
[101] A. Asefnejad, M.T. Khorasani, A. Behnamghader, B. Farsadzadeh, S. Bonakdar, Manufacturing of biodegradable polyurethane scaffolds based on polycaprolactone using a phase separation method: physical properties and in vitro assay, Int. J. Nanomedicine 6 (2011) 2375–2384, https://doi.org/10.2147/ijn.S15586.
[102] Y. Wang, P. Li, L. Kong, Chitosan-modified PLGA nanoparticles with versatile surface for improved drug delivery, AAPS PharmSciTech 14 (2013) 585–592, https://doi.org/10.1208/s12249-013-9943-3.
[103] S. Thomopoulos, W.C. Parks, D.B. Rifkin, K.A. Derwin, Mechanisms of tendon injury and repair, J. Orthop. Res. 33 (2015) 832–839, https://doi.org/10.1002/jor.22806.
[104] J. Buschmann, G. Puippe, G.M. Bürgisser, E. Bonavoglia, P. Giovanoli, M. Calcagni, Correspondence of high-frequency ultrasound and histomorphometry of healing rabbit Achilles tendon tissue, Connect. Tissue Res. 55 (2014) 123–131, https://doi.org/10.3109/03008207.2013.870162.
[105] V. Tan, A. Nourbakhsh, J. Capo, J.A. Cottrell, M. Meyenhofer, J.P. O'Connor, Effects of nonsteroidal anti-inflammatory drugs on flexor tendon adhesion, J. Hand. Surg. [Am.] 35 (2010) 941–947, https://doi.org/10.1016/j.jhsa.2010.02.033.